Cell Communication and Signaling

RESEARCH

Open Access

DOT1L protects against podocyte injury in diabetic kidney disease through phospholipase C-like 1

Yepeng Hu[1†], Shu Ye[1†], Jing Kong[1†], Qiao Zhou[1], Zhe Wang[1], Yikai Zhang[1], Han Yan[1], Yaqiong Wang[1], Tiekun Li[3], Yi Xie[1], Bingbing Chen[4], Yiming Zhao[1], Tianyue Zhang[1], Xianan Zheng[1], Junjia Niu[2], Bibi Hu[4], Shengyao Wang[1], Zhida Chen[2*] and Chao Zheng[1*]

Abstract

Background Podocyte injury causes proteinuria and accelerates glomerular sclerosis during diabetic kidney disease (DKD). Disruptor of telomeric silencing 1-like (DOT1L), an evolutionarily conserved histone methyltransferase, has been reported in preventing kidney fibrosis in chronic kidney disease models. However, whether DOT1L exerts beneficial effects in diabetes induced podocyte injury and the underlying molecular mechanisms need further exploration.

Methods The expression of DOT1L was confirmed by Western blotting in MPC-5 cells and cortex of kidney from *db/db* mice, as well as immunofluorescence staining in human renal biopsy samples. The effect of DOT1L on podocyte injury was obtained using MPC-5 cells and *db/db* mice. The potential target genes regulated by DOT1L was measured by RNA-sequencing. Then, a series of molecular biological experiments was performed to investigate the regulation of PLCL1 by DOT1L in MCP-5 cells and *db/db* mice. Lipid accumulation was assessed by UPLC-MS/MS analysis and Oil Red O staining.

Results DOT1L expression was significantly declined in high glucose (HG)-treated MPC-5 cells, podocyte regions of kidney tissues from *db/db* mice and human renal biopsy samples. Subsequent investigations revealed that upregulation of DOT1L ameliorated HG-induced cell apoptosis in MPC-5 cells as well as primary podocytes. Furthermore, podocyte-specific DOT1L overexpression inhibited diabetic podocyte injury in *db/db* mice. Mechanistically, we revealed that DOT1L upregulated phospholipase C-like 1 (PLCL1) expression by mediating H3K79me2 at its promoter and PLCL1 silencing suppressed the protective role of DOT1L on podocyte injury. Moreover, DOT1L improved diabetes induced abnormal fatty acid metabolism in podocytes and PLCL1 knockdown reversed its protective effects.

†Yepeng Hu, Shu Ye and Jing Kong contributed equally to this work.

*Correspondence:
Zhida Chen
2316066@zju.edu.cn
Chao Zheng
chao_zheng@zju.edu.cn

Full list of author information is available at the end of the article

Conclusions Taken together, our results indicate that DOT1L protects podocyte injury via PLCL1-mediated fatty acid metabolism and provides new insights into the therapeutic target of DKD.

Keywords DOT1L, Diabetic kidney disease, Podocyte injury, PLCL1, Fatty acid metabolism

Background

Diabetic kidney disease (DKD), the leading cause of chronic renal disease (CKD) and end-stage renal disease (ESRD), is among the worst microvascular complications of diabetes [1, 2]. The prevalence of DKD has increased considerably, which parallels the growing trend of diabetes worldwide [3, 4]. It is predicted that the prevalence of diabetes will grow to 642 million in 2040, and 30–40% of them may finally develop DKD, imposing a huge burden on morbidity, mortality, and health expenditure [5]. However, no specific approach has been established yet for DKD treatment. Although current DKD treatment include tightly serum glucose and lipid levels control, renin-angiotensin system (RAS) inhibition, as well as sodium-glucose co-transporter 2 inhibitors (SGLT2is) and mineralocorticoid receptor antagonist (MRA) utilization, the progression of DKD cannot be entirely halted [6–9]. Thus, the specific targets and new therapies on DKD are urgently needed.

Podocyte, a kind of highly differentiated epithelial cell type, is an essential component of the glomerular filtration barrier [10]. Podocyte injury has been considered as a critical event for the onset and progression of DKD [11, 12]. Diabetic podocytes are vulnerable to stressors that cause foot process effacement, podocyte apoptosis, and glomerular sclerosis. An impaired glomerular filtration barrier attributed to podocyte injury causes elevated albumin excretion [13]. A considerable number of patients suffering from DKD develop albuminuria before abnormal serum kidney function indicators [14]. However, the specific and effective therapeutic options to prevent podocyte damage are still absent [13, 15]. The mechanisms of podocyte injury in DKD must be clarified urgently to identify potential therapeutic targets.

Disruptor of telomeric silencing 1-like (DOT1L) is an evolutionarily conserved histone methyltransferase specific for lysine 79 of histone H3 (H3K79) [16, 17]. DOT1L catalyzes mono-, di- and trimethylation of H3K79 (H3K79me1, H3K79me2, and H3K79me3) to regulate transcription elongation, telomere silencing and the DNA repair response [18–20]. Previous studies have uncovered a critical role for DOT1L in driving the pathogenesis of mixed lineage leukemia (MLL)-rearranged leukemia by associating MLL fusion proteins [21–23]. Moreover, recent studies have demonstrated that DOT1L is also involved in solid tumors like neuroblastoma, colorectal cancer, breast cancer, ovarian cancer and prostate cancer [24–28]. Furthermore, DOT1L participates in kidney organogenesis and regulates fibrotic pathways in different renal disease models [29–32]. However, the role of DOT1L in podocyte injury under DKD is yet to be delineated.

In this study, we explored the pivotal role and underlying mechanism of DOT1L in preventing podocyte injury under DKD. Our results revealed decreased DOT1L expression in subjects and mice with DKD and podocytes treated with HG. Furthermore, DOT1L overexpression ameliorated podocyte injury under diabetic conditions in vitro and in vivo. We identified phospholipase C-like 1 (PLCL1) as the downstream target, which was regulated by DOT1L to alleviate podocyte lipid metabolism and resist damage. These results indicate the pivotal role of DOT1L in protecting podocyte function and provide new insights for DKD treatment by targeting DOT1L.

Materials and methods

Human renal biopsy samples

Renal biopsies have been developed as a routine clinical investigation for diagnosing various kidney diseases. The renal biopsy samples were obtained from the Department of Nephrology, The Second Affiliated Hospital of Zhejiang University School of Medicine. Normal control samples were obtained from paracarcinoma tissues of individuals who underwent tumor nephrectomies without diabetes or other kidney disease. The investigations were performed following the principles of the Declaration of Helsinki and approved by the Research Ethics Committee of The Second Affiliated Hospital of Zhejiang University School of Medicine (2023−1098), and informed consent was acquired from the subjects.

Cell Culture and treatments

The conditionally immortalized murine podocyte cell line (MPC-5) was a kind gift from Prof. Chun Zhang (Department of Nephrology, Union Hospital, Tongji Medical College, Huazhong University of Science and Technology, China). MPC-5 cells were cultured in Roswell Park Memorial Institute 1640 medium (RPMI 1640; Gibco, Grand Island, NY, USA) supplemented with 10% fetal bovine serum (FBS; Gibco, Grand Island, NY, USA), 10 U/mL recombinant interferon-γ (IFN-γ; Sigma-Aldrich, St. Louis, USA) and 1% penicillin and streptomycin (Gibco, Grand Island, NY, USA) at 33 °C with 5% CO_2 for proliferation. While reaching appropriate confluence, MPC-5 cells were cultured at 37 °C in 5% CO_2 without IFN-γ for 14 days to induce differentiation.

We isolated primary podocytes from C57BL/6J mice (GemPharmatech Company, Jiangsu, China) as

previously described [33]. Briefly, mice were perfused with 8×10^7 Dynabeads (Thermo Fisher Scientific, Waltham, MA, USA) diluted in 40 mL phosphate-buffered saline (PBS) to harvest the glomeruli. The glomeruli were then filtered through a 100 μm cell strainer (Sigma-Aldrich, St. Louis, USA) and plated on type 1 collagen-coated plates (Thermo Fisher Scientific, Waltham, MA, USA) at 37 °C. Purity was detected by immunofluorescence staining of podocyte-specific markers (Nephrin and Synaptopodin).

We exposed differentiated MPC-5 cells or primary podocytes to high glucose (HG, 30 mmol/L, Sigma-Aldrich, St. Louis, United States USA) for a certain time to induce cellular injury. At the same time, the medium contained normal glucose (NG, 5.6 mmol/L) as a control. Simultaneously, we used MPC-5 cells treated with NG plus mannitol (MA, 24.4 mmol/L, Sigma-Aldrich, St. Louis, United States USA) to eliminate osmotic pressure effects.

To determine whether PPARα play a vital role in PLCL1-mediated fatty acid metabolism, GW6471 (10 μmol/L, MCE, Shanghai, China) was conducted to treat MPC-5 cells.

Gene overexpression and RNA interference of podocyte

Lentivirus expressing DOT1L were obtained from Genepharma (Shanghai, China) and transfected into MPC-5 cells and primary podocytes to overexpress DOT1L. Short interfering RNA (siRNA) sequence targeting PLCL1 were obtained from Genepharma (Shanghai, China) and delivered into MPC-5 cells by Lipofectamine 2000 (Invitrogen, Carlsbad, CA) following the manufacturer's protocol.

Cell viability measurement

Approximately 1×10^4 MPC-5 cells were seeded into 96-well plates with 100 μL medium per well. Then, MPC-5 cells transfected by lentivirus or delivered by siRNA were cultivated in NG or HG medium for 48 h. We performed a cell viability assay with the Cell Counting Kit-8 (CCK-8, Dojindo, Kumamoto, Japan) according to the manufacturer's protocol.

Flow cytometry

MPC-5 cells (approximately 1×10^6 cells/well) at 12-well plates were transfected with corresponding lentivirus and siRNA, then cultivated in NG or HG medium for 48 h. Subsequently, cell apoptosis was detected by the Annexin V-FITC/ (PI) Apoptosis Detection Kit (BD, USA) following the manufacturer's protocol. FITC- and PI-stained cells were assessed using a CytoFlex flow cytometer (Beckman Coulter, USA). The cell apoptosis data were analyzed by Flowjo software (version 10, Tree Star, USA).

mRNA library construction and sequencing

Total RNA was isolated and purified using TRIzol reagent (Invitrogen, Carlsbad, CA, USA) following the manufacturer's procedure. The RNA amount and purity of each sample was quantified using NanoDrop ND-1000 (NanoDrop, Wilmington, DE, USA). The RNA integrity was assessed by Bioanalyzer 2100 (Agilent, CA, USA) with RIN number > 7.0, and confirmed by electrophoresis with denaturing agarose gel. Poly (A) RNA is purified from 1 μg total RNA using Dynabeads Oligo (dT)25-61005 (Thermo Fisher, CA, USA) using two rounds of purification. Then the poly(A) RNA was fragmented into small pieces using Magnesium RNA Fragmentation Module (NEB, Cat No. e6150, USA) under 94℃ 5–7 min. Then the cleaved RNA fragments were reverse-transcribed to create the cDNA by SuperScript™ II Reverse Transcriptase (Invitrogen, Cat No. 1896649, USA), which were next used to synthesise U-labeled second-stranded DNAs with E. coli DNA polymerase I (NEB, Cat No.m0209, USA), RNase H (NEB, Cat No.m0297, USA) and dUTP Solution (Thermo Fisher, Cat No. R0133, USA). An A-base is then added to the blunt ends of each strand, preparing them for ligation to the indexed adapters. Each adapter contains a T-base overhang for ligating the adapter to the A-tailed fragmented DNA. Single- or dual-index adapters are ligated to the fragments, and size selection was performed with AMPureXP beads. After the heat-labile UDG enzyme (NEB, Cat No. m0280, USA) treatment of the U-labeled second-stranded DNAs, the ligated products are amplified with PCR by the following conditions: initial denaturation at 95℃ for 3 min; 8 cycles of denaturation at 98℃ for 15 s, annealing at 60℃ for 15 s, and extension at 72℃ for 30 s; and then final extension at 72℃ for 5 min. The average insert size for the final cDNA library was 300±50 bp. At last, we performed the 2×150 bp paired-end sequencing (PE150) on an Illumina Novaseq™ 6000 (LC-Bio Technology CO., Ltd., Hangzhou, China) following the vendor's recommended protocol.

Sequence and primary analysis

Cutadapt software was used to remove the reads that contained adaptor contamination. And after removed the low-quality bases and undetermined bases, we used HISAT2 software to map reads to the genome. The mapped reads of each sample were assembled using StringTie with default parameters. Then, all transcriptomes from all samples were merged to reconstruct a comprehensive transcriptome using gffcompare software. After the final transcriptome was generated, StringTie and ballgown were used to estimate the expression levels of all transcripts and perform expression level for mRNAs by calculating FPKM. The differentially expressed mRNAs were selected with fold change > 2 or

fold change < 0.5 and adjusted P value < 0.05, and then analysis GO enrichment and KEGG enrichment to the differentially expressed mRNAs.

Chromatin immunoprecipitation (ChIP)

The ChIP assay was performed as described previously [34]. Briefly, cells were crosslinked with 1% formaldehyde, then quenched using 125 mM glycine, washed with cold PBS, and collected in a tube. Samples were lysed with 10 mM Hepes, 1.5 mM $MgCl_2$, 10 mM KCl, and 0.4% NP-40 containing a 1× protein inhibitor cocktail. Then, after centrifuging the samples, the supernatant was discarded. The precipitate was resuspended with 50 mM Tris HCl (pH 7.4), 2.5 mM EDTA, 0.2% Triton X-100, and 0.5% SDS to lyse the nucleus. The Crosslinked chromatin was fragmented by ultrasound treatment. Chromatin was immunoprecipitated with H3K79me2 antibody (Cell Signaling Technology, Cat No. 5427 S, 1:50) or respective IgG antibody (Abcam, Cat No. ab171870, 1:100). Next, immunoprecipitated DNA was extracted and detected by a quantitative PCR using the input samples as the internal control. The primer sequences of *Plcl1*, *Dppa2* and *Hecw2* used for quantitative PCR were presented in Supplementary Table 1. To identify the specific regions where H3K79me2 enriched, the *Plcl1* promoter region (ranged from −3000 to 3000 bp) was separated into six parts (1000 bp per part) to cover the promoter area by one set of primers, which were presented in Supplementary Table 2.

Animal studies

All animal study protocols were approved by the Zhejiang Chinese Medical University's Animal Care Committee (20211206-04). Six-week-old male *db/db* (C57BLKS/J-*lepr*^{db}/*lepr*^{db}) and their littermate *db/m* mice were bought from GemPharmatech Company (Jiangsu, China). Mice (3–5 per cage) were housed at 23 ± 1 °C on a 12-h light/12-h dark cycle with free access to food and water. Mice were allocated using the random number method, and investigators were blinded to allocated animals when assessing the experimental outcomes. Animals were acclimatized for two weeks before experimentation.

To induce DOT1L overexpression in glomeruli, AAV9-Nphs1-DOT1L were generated by Genepharma (Shanghai, China). The mice were randomly divided into three groups: (i) *db/m* mice + AAV9-Nphs1-NC (*db/m* + NC); (ii) *db/db* mice + AAV9-Nphs1-NC (*db/db* + NC); (iii) *db/db* mice + AAV9-Nphs1-DOT1L (*db/db* + DOT1L). For knocking down PLCL1 in vivo, AAV9-Nphs1-shPLCL1 were obtained from Genepharma (Shanghai, China). To testify whether PLCL1 was involved in DOT1L-mediated protective effect, mice were randomly divided into four groups: (i) *db/m* mice + AAV9-Nphs1-NC (*db/m* + NC); (ii) *db/db* mice + AAV9-Nphs1-NC (*db/db* + NC); (iii) *db/db* mice + AAV9-Nphs1-DOT1L (*db/db* + DOT1L); (iv) *db/db* mice + AAV9-Nphs1-DOT1L + AAV9-Nphs1-shPLCL1 (*db/db* + DOT1L + shPLCL1). Each mouse received AAV9-Nphs1-DOT1L (5×10^{11} vector genomes) with or without AAV9-Nphs1-shPLCL1 (5×10^{11} vector genomes) treatment by tail-vein injection at eight weeks. At 12 and 16 weeks, each group of mice received the same dose of AAV9 again. The body weight and blood glucose were monitored every two weeks. At 20 weeks, 24-h urine samples, serum samples and kidney tissues were harvested for further study.

Biochemical analysis of serum and urine samples

Blood urea nitrogen (BUN), serum creatinine and 24-h urinary protein were detected using an automatic biochemical analyzer (Hitachi, Tokyo, Japan).

Western blotting

We extracted total protein lysates of cultured MPC-5 cells or renal tissues using the RIPA buffer containing protease and phosphatase inhibitors (Solarbio, Beijing, China). Moreover, total protein concentrations were estimated using the Enhanced BCA Protein Assay Kit (Beyotime, Shanghai, China). Then, equal amounts of total protein were subjected to electrophoresis and transferred onto polyvinylidene difluoride membranes (Millipore, MA, USA). Membranes were blocked in 5% bovine serum albumin (BSA) for 1 h at room temperature. Primary antibodies used as following: H3K79me1(Cell Signaling Technology, Cat No. 12522 S, 1:1000), H3K79me2 (Cell Signaling Technology, Cat No. 5427T, 1:1000), H3K79me3 (Cell Signaling Technology, Cat No. 74073 S, 1:1000), histone H3 (Cell Signaling Technology, Cat No. 4499 S, 1:1000), DOT1L (Abcam, Cat No. ab64077, 1:2000), Nephrin (Abcam, Cat No. ab216341, 1:1000), Caspase-3 (Cell Signaling Technology, Cat No. 9662 S, 1:1000), PLCL1 (Novus Biologicals, Cat No. NBP2-94627, 1:500), Hecw2 (GeneTex, Cat No. GTX33989, 1:500), Dppa2 (Abcam, Cat No. ab91318, 1:1000), FASN (Abcam, Cat No. ab128870, 1:1000), ACC1 (Abcam, Cat No. ab45174, 1:1000), SCD1 (Cell Signaling Technology, Cat No. 2794 S, 1:1000), CPT1a (Abcam, Cat No. ab 128568, 1:1000), PPARα (ABclonal, Cat No. A25296, 1:1000), β-actin (Abways, Cat No. AB0035, 1:2000). The immunoreactive bands were then detected with corresponding horseradish peroxidase-conjugated secondary antibodies (Yeasen, Shanghai, China) and visualized using enhanced chemiluminescent reagents (Cyanagen, Bologna, Italy). The protein ladders purchased from Coffit (Cat No. LBP6510-10) and Thermo Scientific (Cat No. 26625) were used in this study. Image acquisition was performed using AMERSHAM ImageQuant 800. The band densitometry was quantified using ImageJ software (version 1.52a, NIH, USA).

Immunofluorescence staining

Kidney-frozen Sect. (8 μm thick) or cell samples were fixed with 4% paraformaldehyde (PFA) for 15 min and permeabilized using 0.2% Triton X-100 for 10 min at room temperature. After blocking with 5% donkey serum for 30 min at 37 °C, specimens were incubated overnight at 4 °C with primary antibodies: Desmin (Abcam, Cat No. ab32362, 1:200), Nephrin (R&D Systems, Cat No. AF3159, 1:00), Synaptopodin (Synaptic Systems, Cat No. 163004, 1:200). For immunofluorescent double-staining, sections were incubated overnight at 4 °C with both Synaptopodin (Synaptic Systems, Cat No. 163004, 1:200) and Cleaved Caspase-3 (Cell Signaling Technology, Cat No. 9664 S, 1:200) or Adipophilin (Proteintech, Cat No.15294-1-AP, 1:200). These slides were treated with corresponding Alexa Fluor labeled secondary antibodies (Abcam) at room temperature for 1 h after washing. The images were captured by a fluorescence microscope (Zeiss, Oberkochen, Germany) or confocal microscope (Fluoview FV1000, Olympus, Japan). The fluorescence intensity was quantified using ImageJ software (version 1.52a, NIH, USA). Image Pro Plus software (version 6.0, Bethesda, MD) was used to analyze colocalization and quantified as the Pearson correlation coefficient.

Immunohistochemistry

Renal biopsy kidney tissues were fixed in 4% PFA, embedded in paraffin and sectioned at 4 μm thickness. Deparaffinized and rehydrated sections were blocked with 5% BSA for 30 min at room temperature and incubated overnight at 4 °C with the primary antibodies for H3K79me2 (Abcam, Cat No. ab3594, 1:100). Sections were washed with PBS to remove excessive staining and incubated with horseradish peroxidase-conjugated secondary antibody (Yeasen, Shanghai, China). Positive staining was visualized by a DAB developing system (Beyotime, Shanghai, China). Finally, sections were counterstained with hematoxylin and observed by light microscopy (Nikon, Tokyo, Japan).

Morphological examination

Mouse kidney tissues were fixed in 4% PFA, embedded in paraffin and cross-sectioned (4 μm) for morphological examination. Paraffin sections were stained with periodic-acid-schiff (PAS) using standard procedures. Images were taken with a light microscope (Nikon, Tokyo, Japan).

Mesangial area was quantified per glomerulus area using ImageJ software (version 1.52a, NIH, USA) [35]. Glomerular damage index (GDI) was scored semi-quantitatively as previously described [36, 37]. Briefly, at least 20 glomeruli per mouse were measured and classified from 0 to 4 based on the percentage of damaged glomerular area occupying the respective glomerulus: 0, 0%; 1, <25%; 2, 25 to 50%; 3, 50 to 75%; and 4, >75%. GDI was calculated as the following formula: $(n1\times0) + (n2\times1) + (n3\times2) + (n4\times3) + (n5\times4)/N$, whereby n1 to n5 represented the numbers of glomeruli with respective scores of 0–4 and $N=n1+n2+n3+n4+n5$.

Quantitative real-time reverse transcription PCR (RT-qPCR)

Total RNA was isolated from MPC-5 cells by TRIzol reagent (Invitrogen, Carlsbad, CA) and 1 μg of total RNA was reversed transcribed into cDNA using the PrimeScript RT reagent Kit (Takara, Japan). Quantitative real-time PCR was performed using the SYBR green fluorescent dye mix (Yeasen, Shanghai, China). β-actin was used as the normalization control. Relative mRNA levels were calculated using the $2^{-\Delta\Delta}$Ct method and sequences of primers used for qPCR were listed in Supplementary Table 3.

UPLC-MS/MS analysis

MPC-5 cell samples from different groups were collected for lipidomic analysis. Cells pellets containing at least 1×10^6 cells per sample were subjected to liquid extraction. UPLC-MS/MS analysis was performed at DURNRAIN (Hangzhou, China).

Oil Red O staining and Nile red staining

For Oil Red O staining, frozen sections of the kidney (8 μm thick) were dried at room temperature for 10 min. MPC-5 cells were cultured on coverslips and fixed with 4% PFA for 20 min. The frozen sections or coverslips were washed with PBS and soaked into 60% isopropanol thrice and then stained with 0.3% Oil Red O dye solution (Sigma-Aldrich, St. Louis, USA) for 10 min, and excessive staining was removed by washing with 60% isopropanol. The frozen sections or coverslips were counterstained in hematoxylin for 1 min. Then, washed sections or coverslips were photographed under a microscope (Nikon, Tokyo, Japan).

For Nile red staining, MPC-5 cells cultured on round coverslips were fixed with 4% PFA, rinsed with PBS and stained with 0.05 mg/mL Nile red solution for 10 min. Then, cell nuclei were counterstained with DAPI. Images were acquired by a confocal microscope (Fluoview FV1000, Olympus, Japan).

Statistical analysis

We performed 2-tailed Student's *t* test, 1-way ANOVA with Dunnett's post hoc test, and 2-way ANOVA with Bonferroni's post hoc test to assess statistical significance using GraphPad Prism 7 (San Diego, CA, USA). The results are presented as the mean±SEM. All experiments were repeated at least in triplicate, and representative experiments are shown. $P<0.05$ was statistically significant.

Results

DOT1L expression was downregulated in HG-treated podocytes, rodent diabetic kidney tissues and human renal biopsy samples

We first examined DOT1L protein levels in HG-induced MPC-5 cells. Western blotting analysis showed that the protein level of DOT1L expression was significantly downregulated after HG treatment in a time dependent manner. Mannitol was added in the medium for 48 h as the osmotic pressure control for HG, which did not affect DOT1L expression (Fig. 1A). Previous studies reported that DOT1L was a specific methyltransferase of H3K79 [16]; thus, we tested H3K79me1/2/3 levels in HG-induced MPC-5 cells. As expected, H3K79me1/2/3 levels were significantly decreased in HG-treated MPC-5 cells (Fig. 1B). Additionally, DOT1L expression and H3K79me1/2/3 levels were significantly decreased in the renal cortex of *db/db* mice compared with *db/m* mice (Fig. 1C and D). Of note, both in vivo and in vitro experiments showed a more pronounced decrease for the H3K79me2 compared with H3K79me1/3 (Fig. 1B and D). Immunofluorescence co-staining revealed that the DOT1L expressions were declined in podocyte regions of *db/db* mice and renal biopsy samples obtained from subjects with DKD (Fig. 1E-G). Moreover, H3K79me2 was decreased in glomeruli of DKD patients as evidenced by immunohistochemical staining (Fig. S1A). These findings indicate that the expression of DOT1L is decreased greatly in podocyte under diabetic conditions.

DOT1L protected against HG-induced podocyte injury

To evaluate the role of DOT1L in the progression of diabetes induced podocyte injury, DOT1L was overexpressed in MPC-5 cells by lentivirus transfection and the transfection efficiency was confirmed by Western blotting (Fig. 2A). Meanwhile, HG treatment caused podocyte injury indicated by the suppressed expression of podocyte marker Nephrin, which was recovered by DOT1L overexpression (Fig. 2B). Consistently, we also detected the expression of Desmin, a classic podocyte injury marker, by immunofluorescence staining. DOT1L overexpression significantly diminished the upregulated expression of Desmin after HG treatment (Fig. 2C). Hyperglycemia has been reported to restrain cell viability and induce podocyte apoptosis [38]. In our present study, we observed that DOT1L overexpression significantly improved cell viability and ameliorated podocyte apoptosis (Fig. 2D and E).

Subsequently, in order to further examined the protective role of DOT1L in the podocytes, we extracted the primary podocytes from mouse glomeruli which were confirmed by podocyte-specific markers for Nephrin and Synaptopodin (Fig. S2A). Consistent with the results in MPC-5 cells, HG stimulation inhibited DOT1L expression in primary podocytes and DOT1L overexpression reversed HG-induced decline of Nephrin expression and prevented podocyte apoptosis (Fig. S2B–F). Overall, these data suggest the protective effects of DOT1L in preventing HG-induced podocyte injury.

Podocyte-specific DOT1L overexpression ameliorated podocyte injury of *db/db* mice

Then we embarked on investigating whether increased DOT1L expression in podocyte could attenuate diabetic podocyte injury in vivo. DOT1L overexpression was induced by tail-vein injection of AAV9 expressing DOT1L driving by Nphs1 (the podocyte specific promotor) monthly. Western blotting analysis showed that DOT1L was overexpressed successfully in the renal cortex of *db/db* mice (Fig. 3A). Furthermore, glomeruli were isolated to assess the expression of DOT1L (Fig. 3B). Compared to *db/db* mice injected with control AAV9, the mRNA level of DOT1L was increased significantly in the glomeruli of DOT1L overexpressing-AAV9 transfected *db/db* mice, as well as the expression of DOT1L in glomeruli as evidenced by immunofluorescence staining (Fig. 3C and D). DOT1L overexpression did not affect the blood glucose and body weight in *db/db* mice (Fig. S3A and B). Of note, serum creatinine, serum BUN and 24-h urinary protein was decreased after DOT1L overexpression (Fig. 3E). PAS staining revealed that *db/db* mice exhibited obvious glomerular hypertrophy and mesangial expansion and scored higher glomerular damage index (GDI) compared with the *db/m* mice, which was reversed by DOT1L overexpression (Fig. 3F and G). Subsequently, podocyte injury was examined. Podocyte number reflected by WT1 immunohistochemical staining revealed that DOT1L overexpression ameliorated podocyte loss in *db/db* mice (Fig. 3H). Meanwhile, the loss of Nephrin in glomeruli of *db/db* mice was alleviated by DOT1L overexpression (Fig. 3I). Correspondingly, the protein level of Nephrin was reinstated in *db/db* mice after DOT1L overexpressing-AAV9 transfection, in comparison to *db/db* mice treated with the control AAV9 (Fig. 3J). Moreover, the colocalized signal of Cleaved Caspase-3 with the marker of the podocyte (Synaptopodin) was enhanced in *db/db* mice, while DOT1L overexpressing reversed these effects (Fig. 3K). Above data suggest that DOLT1 protects against diabetes induced renal function deterioration and podocyte injury in vivo.

DOT1L upregulated PLCL1 expression by mediating H3K79me2 at its promoter

RNA-sequencing was performed to unravel the genes regulated by DOT1L overexpression following HG treatment in MPC-5 cells. A total of 556 differentially expressed genes were identified between NG+Vec and HG+Vec group, and 559 differentially expressed genes

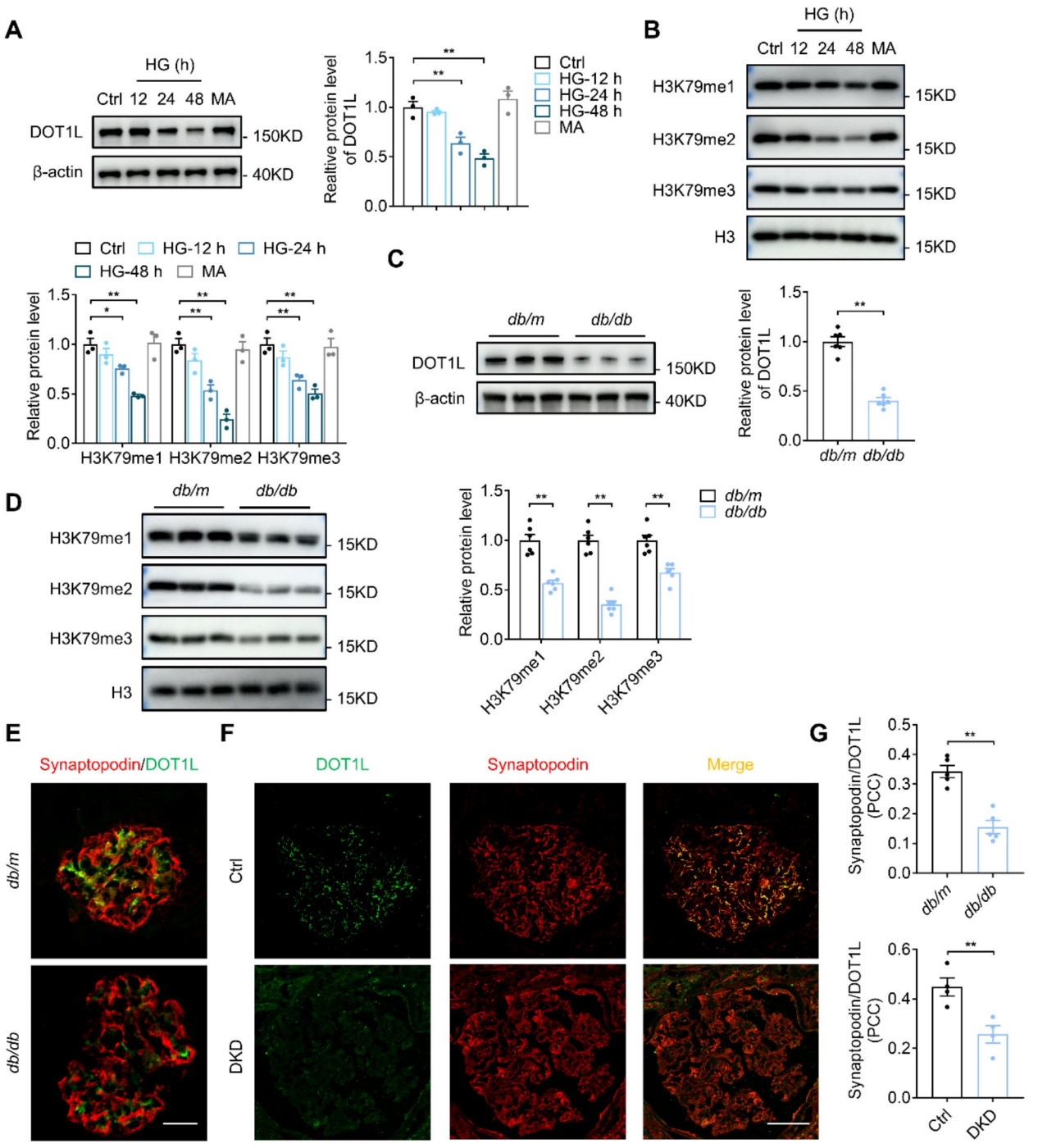

Fig. 1 DOT1L expression was down-regulated in HG-treated podocytes, rodent diabetic kidney tissues and human renal biopsy samples. **A** Representative Western blotting and quantification of DOT1L in MPC-5 cells treated with high glucose (HG, 30 mmol/L) in a time-dependent manner ($n=3$ per group). **B** Representative Western blotting and quantification of H3K79me1/2/3 in MPC-5 cells treated with HG in a time-dependent manner ($n=3$ per group). **C** Representative Western blotting and quantification of DOT1L in the renal cortex of *db/m* and *db/db* mice ($n=6$ per group). **D** Representative Western blotting and quantification of H3K79me1/2/3 in the renal cortex of *db/m* and *db/db* mice ($n=6$ per group). **E** Representative immunofluorescence co-staining images between Synaptopodin (red) and DOT1L (green) in kidney tissues of mice ($n=5$ per group). Scale bar, 25 μM. **F** Representative immunofluorescence co-staining images between Synaptopodin (red) and DOT1L (green) in renal biopsy samples obtained from subjects with or without DKD ($n=4$ per group). Scale bar, 50 μM. **G** The summarized colocalization coefficient for E and F. Data are presented as the mean ± SEM. $^{*}P<0.05$, $^{**}P<0.01$

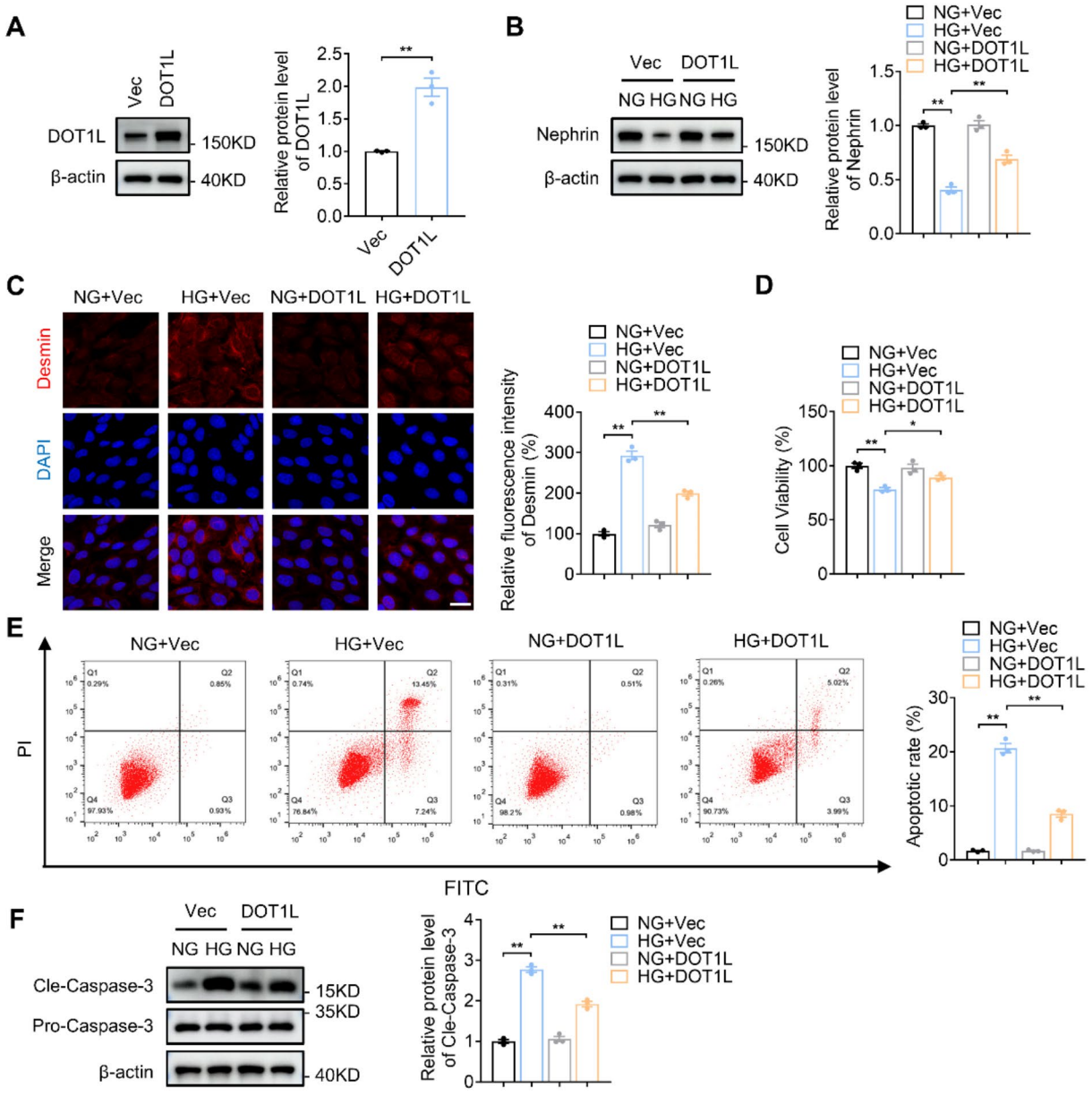

Fig. 2 DOT1L overexpression ameliorated HG-induced podocyte injury *in vitro*.**A** Representative Western blotting and quantification of DOT1L in MPC-5 cells with or without DOT1L overexpression ($n=3$ per group). **B** Representative Western blotting and quantification of Nephrin in MPC-5 cells treated with DOT1L-lentivirus and HG stimulation ($n=3$ per group). **C** Representative immunofluorescence staining of Desmin in MPC-5 cells under different treatment approaches ($n=3$ per group). Scale bar, 25 μm. **D** Cell Viability of MPC-5 cells under different treatment approaches ($n=3$ per group). **E** Level of apoptosis of MPC-5 under different treatment approaches detected by flow cytometry ($n=3$ per group). **F** Representative Western blotting and quantification of Cleaved Caspase-3 in MPC-5 cells under different treatment approaches ($n=3$ per group). Data are presented as mean ± SEM. $^{*}P<0.05$, $^{**}P<0.01$. cle-Caspase-3: Cleaved Caspase-3

were identified between HG+Vec and HG+DOT1L group (Fig. S4A and B). Previous studies have reported that DOT1L is enriched in actively transcribing genes and promotes target gene expression [16]. Thus, we hypothesized that DOT1L overexpression upregulated genes associated with defense of podocyte injury. We focused on genes which were downregulated in HG-treated podocytes, while upregulated after DOT1L overexpression, and sixteen overlapped genes were finally filtered (Fig. S4C). As shown in Fig. 4A, *Plcl1*, *Dppa2* and *Hecw2* were the most significant genes. Then we confirmed by Western blotting that HG treatment decreased PLCL1, Dppa2 and Hecw2 protein levels, however, DOT1L overexpression only reversed PLCL1 expression (Fig. 4B and C). It has been reported that DOT1L regulates gene expression by augmenting H3K79

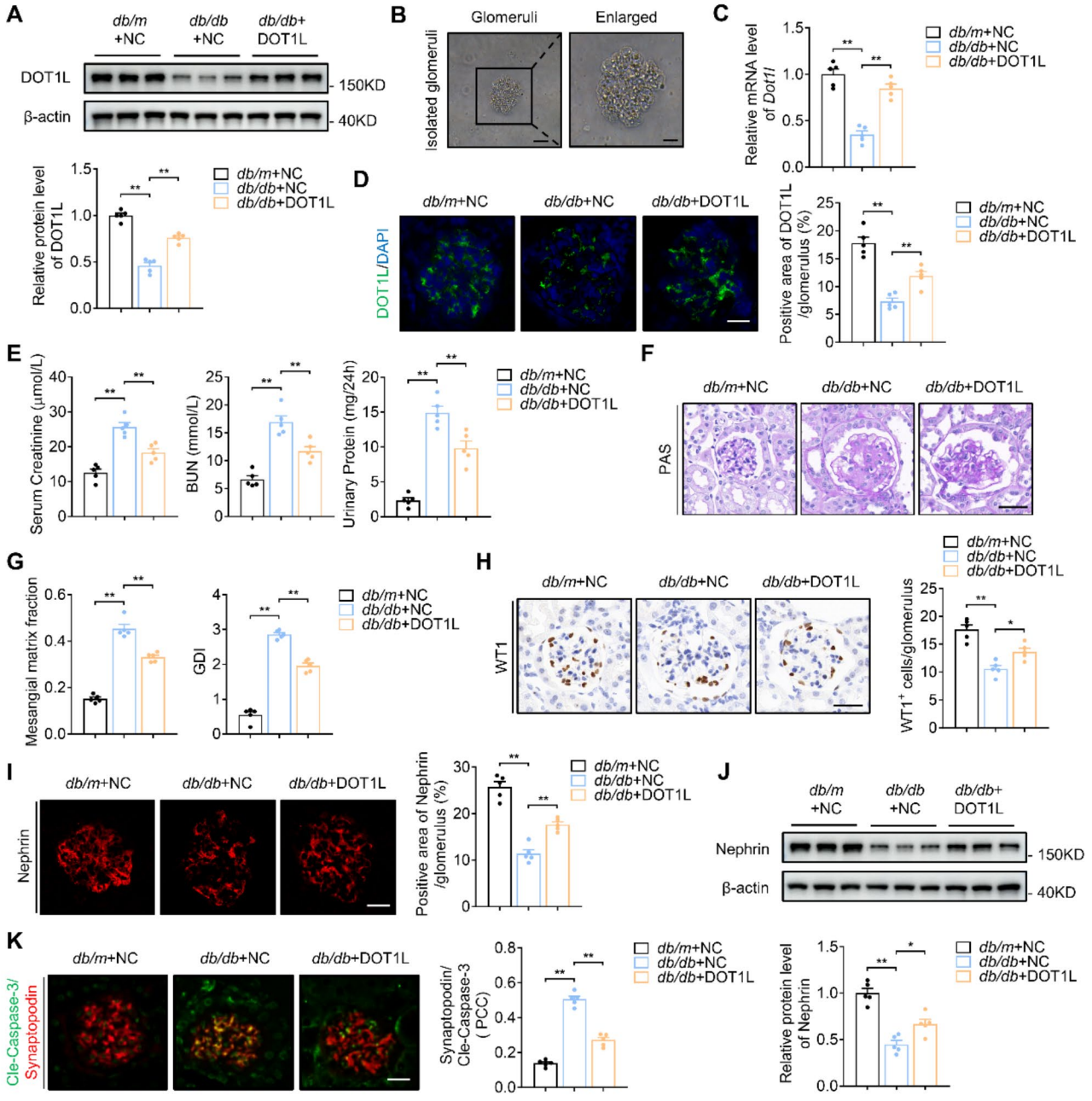

Fig. 3 DOT1L overexpression ameliorated diabetes induced podocyte injury in *db/db* mice. **A** Representative Western blotting and quantification of DOT1L in renal cortex of mice at 20 weeks from different groups ($n = 5$ per group). **B** Isolated glomeruli captured by microscopy. Scale bar, 50 μm (left), 25 μm (right). **C** The relative mRNA level of *Dot1l* in isolated glomeruli ($n = 5$ per group). **D** Representative immunofluorescence staining images of DOT1L (green). ($n = 5$ per group). Scale bar, 20 μm. **E** Serum creatinine, BUN and 24-h urinary protein of mice from different groups ($n = 5$ per group). **F** Representative images of morphological changes from periodic acid-Schiff (PAS) staining ($n = 5$ per group). Scale bar, 20 μm. **G** Quantification of the percentage of mesangial matrix area and glomerular damage index (GDI) ($n = 5$ per group). **H** Representative photomicrographs and quantification of WT1 showed the number of podocytes in each glomerular. ($n = 5$ per group). Scale bar, 20 μm. **I** Representative immunofluorescence staining of Nephrin and the quantitative analysis in the kidney from different groups ($n = 5$ per group). Scale bar, 20 μm. **J** Representative Western blotting and quantification of Nephrin in renal cortex of mice from different groups ($n = 5$ per group). **K** Representative immunofluorescence co-staining (yellow) between Synaptopodin (red) and Cle-Caspase-3 (green) and the summarized colocalization coefficient ($n = 5$ per group). Scale bar, 20 μm. Data are presented as mean ± SEM. $^{*}P < 0.05$, $^{**}P < 0.01$. cle-Caspase-3: Cleaved Caspase-3. *db/m* + NC: *db/m* mice + AAV9-Nphs1-NC, *db/db* + NC: *db/db* mice + AAV9-Nphs1-NC, *db/db* + DOT1L: *db/db* mice + AAV9-Nphs1-DOT1L

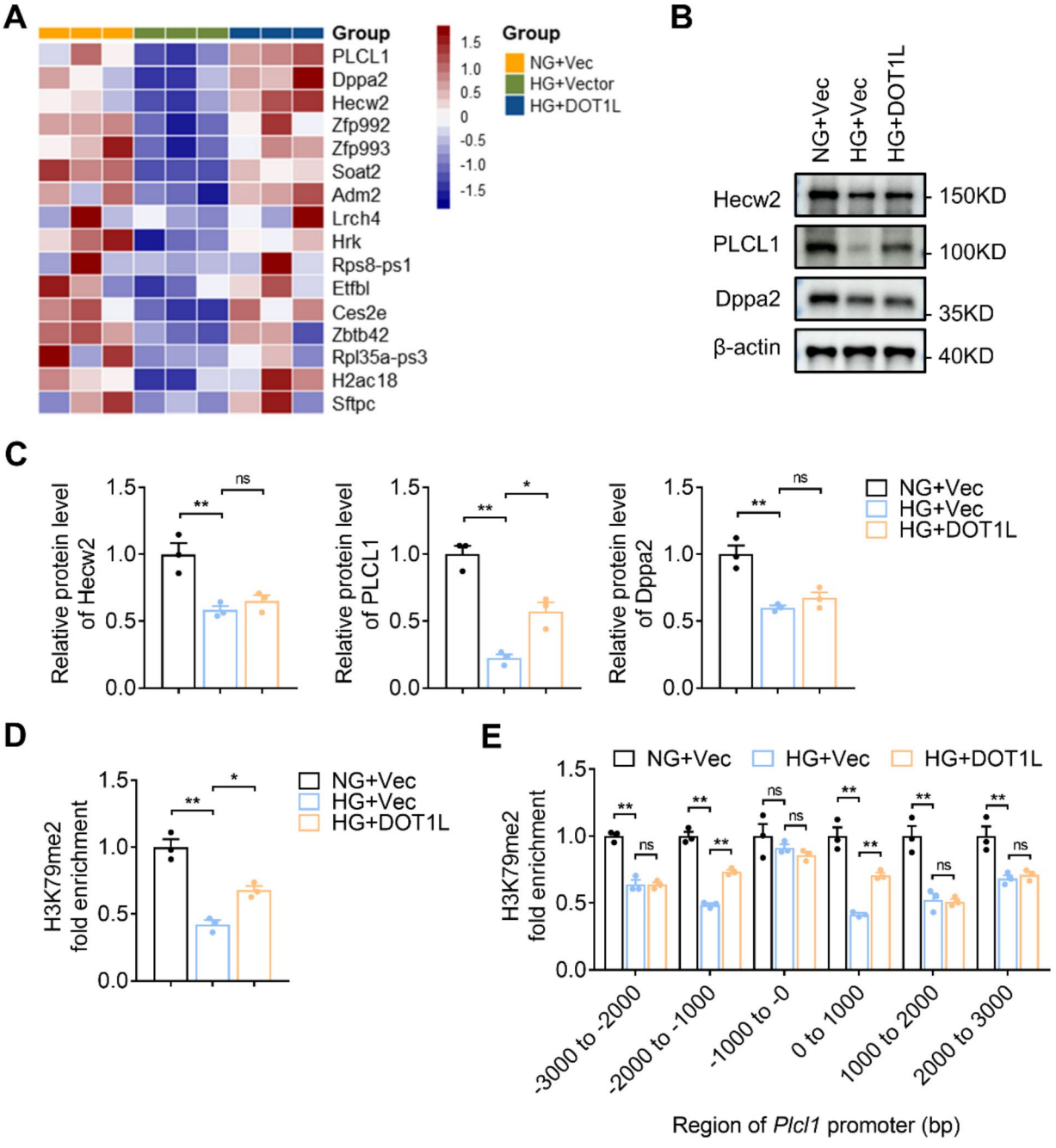

Fig. 4 DOT1L upregulated PLCL1 expression by mediating H3K79me2 at its promoter. **A** Heatmap of 16 overlapped genes among three groups ($n=3$ per group). **B**, **C** Representative Western blotting and quantification of PLCL1, Hecw2 and Dppa2 in MPC-5 cells from different groups ($n=3$ per group). **D** ChIP-qPCR analysis of H3K9me2 levels at the promoters of *Plcl1* in MPC-5 cells from different groups ($n=3$ per group). **E** ChIP-qPCR analysis of H3K9me2 levels at various promoter regions of *Plcl1* in MPC-5 cells from different groups ($n=3$ per group). Data are presented as mean ± SEM. *$P<0.05$, **$P<0.01$. ns: not significantly different

methylation at gene promoters [17]; thus, we proceeded to investigate whether DOT1L could directly regulate promoter methylation levels on *Plcl1*, *Dppa2* and *Hecw2*. ChIP analysis revealed that HG treatment repressed H3K79me2 levels in the *Plcl1* promoter regions, which was reversed by DOT1L overexpression (Fig. 4D). However, HG treatment with or without DOT1L overexpression did not significantly affect H3K79me2 levels in the

Dppa2 and *Hecw2* promoter regions (Fig. S4D). Furthermore, we divided the *Plcl1* promoter region into six parts (1000 bp per part) and confirmed that H3K79me2 was regulated by DOT1L in the specific regions (-2000 to -1000 bp, 0–1000 bp) at the *Plcl1* promoters (Fig. 4E). Taken together, these data indicate that DOT1L regulates *Plcl1* expression through augmenting H3K79me2 at its promoters.

DOT1L attenuated podocyte injury under diabetic conditions in PLCL1 dependent way

Then, we testified the indispensable role of PLCL1 in DOT1L-preserved protective effects on podocytes. MPC-5 cells were transfected with PLCL1-siRNA (siPLCL1) to knockdown the PLCL1 and the transfection efficiency was validated by Western blotting (Fig. 5A). Subsequently, we demonstrated the effects of DOT1L overexpression combined with PLCL1 knockdown on podocyte injury after HG treatment. In line with prior findings, DOT1L overexpression restored Nephrin expression, upregulated cell viability, alleviated apoptotic rate, attenuated Cleaved Caspase-3 production in HG-treated podocytes, however, PLCL1 knockdown suppressed the protective role of DOT1L on podocyte injury (Fig. 5B–E). These results above-mentioned suggest that DOT1L prevents HG-induced podocytes injury by upregulating PLCL1.

Next, we further confirmed that DOT1L ameliorated diabetic podocyte injury by promoting PLCL1 expression in *db/db* mice. DOT1L overexpression and PLCL1 depletion were performed in the podocytes of *db/db* mice through tail-vein injection of AAV9 conducted with Nphs1 promotor. Western blotting analysis showed that DOT1L was overexpressed and PLCL1 was knockdown successfully in the renal cortex of *db/db* mice (Fig. 6A). Then glomeruli were isolated and RT-qPCR was performed to further verified the transfection efficiency. mRNA analysis revealed that DOT1L levels were increased and PLCL1 levels were decreased significantly in the glomeruli of AAV9 transfected mice (Fig. 6B). Of note, DOT1L overexpression combined with PLCL1 knockdown did not affect the blood glucose and body weight in *db/db* mice (Fig. S5A and B). DOT1L overexpression significantly decreased serum creatinine, serum BUN and 24-h urinary protein, which was reversed after PLCL1 inhibition (Fig. 6C). Moreover, PAS staining revealed that the attenuation of glomerular mesangial expansion induced by DOT1L overexpression was blunted after PLCL1 knockdown (Fig. 6D and E). Podocyte damage revealed by Nephrin and podocyte number reflected by WT1 in *db/db* mice were recovered by DOT1L overexpression, which was blunted after PLCL1 knockdown (Fig. 6F and G). Moreover, immunofluorescence staining showed that DOT1L overexpression diminished diabetes induced elevation of Cleaved Caspase-3 expression in podocytes, which was abrogated after silencing PLCL1 (Fig. 6H). Overall, these data substantiate the assertion that DOT1L ameliorates podocyte injury by upregulating PLCL1 expression.

DOT1L attenuated podocytes injury under diabetic conditions mainly through promoting PLCL1-mediated fatty acid metabolism

Previous studies have demonstrated that abnormal lipid accumulation is a crucial pathological process for podocyte injury under diabetic conditions [39–41]. Intriguingly, PLCL1 has been found to be involved in lipid metabolism and decrease the amount of lipid droplets [42, 43]. To confirm whether DOT1L regulated lipid metabolism by upregulating PLCL1 expression, we evaluated the effects of DOT1L overexpression combined with PLCL1 knockdown on podocyte lipid accumulation under HG stimuli. As shown by Oil Red O staining and Nile Red staining, HG treatment resulted in remarkable lipid accumulation in MPC-5 cells. DOT1L overexpression reduced lipid droplets in HG-treated MPC-5 cells, which was abrogated after PLCL1 silencing (Fig. 7A). Then we performed ultra performance liquid chromatography tandem mass spectrometry (UPLC-MS/MS)-based lipidomic analysis, and the results demonstrated that the main species of lipid deposition were fatty acids (FA) and triglyceride (TG), but not phosphatidylcholines (PC) and cholesterol esters (CE), indicating that DOT1L primarily regulated fatty acid metabolism through PLCL1 in podocytes (Fig. 7B and C, Fig. S6A and B). Fatty acid metabolism homeostasis was regulated by de novo synthesis, fatty acid uptake and oxidation processes [44]. Therefore, we evaluated the expression of key genes involved in these processes. Our results revealed that DOT1L overexpression restored the upregulated mRNA levels of fatty acid synthesis genes and the reduced fatty acid oxidation genes induced by HG stimuli, which was obviously eliminated by PLCL1 knockdown. However, DOT1L overexpression or PLCL1 knockdown did not significantly affect fatty acid uptake-related gene expression (Fig. 7D). Consistent results were obtained from Western blotting analyses (Fig. 7E). To further determine whether PPARα played a vital role in PLCL1-mediated fatty acid metabolism, GW6471 (specific PPARα inhibitor) was conducted to treat MPC-5 cells. The mRNA analysis revealed that PLCL1 knockdown decreased the mRNA level of *Cpt1a* in MPC-5 cells treated with vehicle, while this effect was blunted by inhibition of PPARα. Moreover, PLCL1 knockdown did not significantly affect the expression of fatty acid uptake related genes both in vehicle groups and GW6471 groups (Fig. S6C).

To clarify the role of DOT1L in podocyte fatty acid metabolism in vivo, we overexpressed DOT1L and

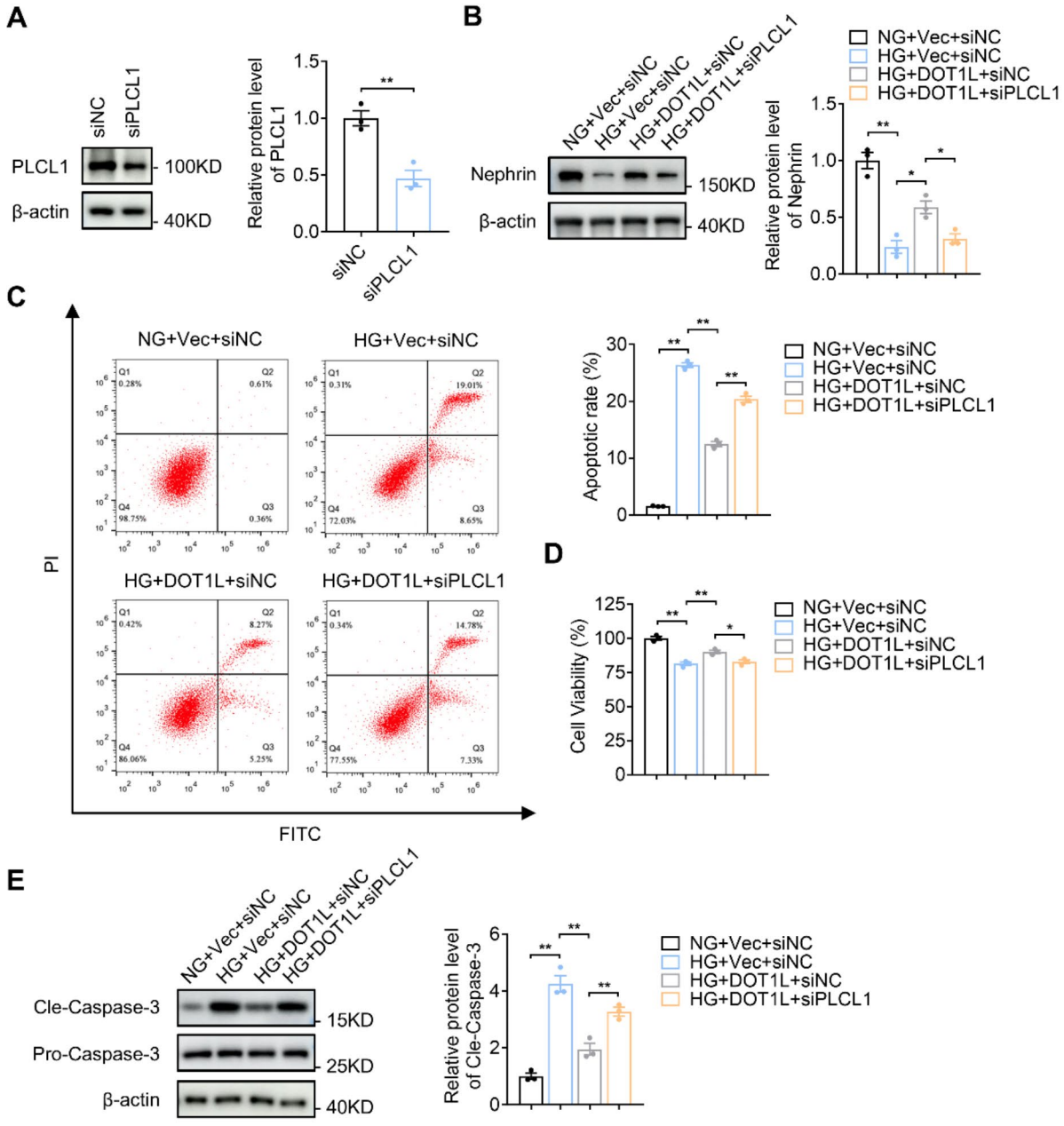

Fig. 5 DOT1L ameliorated the podocyte injury after HG treatment through PLCL1 *in vitro*.**A** Representative Western blotting and quantification of PLCL1 in MPC-5 cells after siPLCL1 transfection ($n=3$ per group). **B** Representative Western blotting and quantification of Nephrin in MPC-5 with DOT1L-lentivirus and siPLCL1 transfection under HG stimulation ($n=3$ per group). **C** Level of apoptosis of MPC-5 under different treatment approaches detected by flow cytometry ($n=3$ per group). **D** Cell Viability of MPC-5 cells under different treatment approaches ($n=3$ per group). **E** Representative Western blotting and quantification of Cleaved Caspase-3 in MPC-5 cells under different treatment approaches ($n=3$ per group). Data are presented as mean ± SEM.*$P<0.05$, **$P<0.01$. cle-Caspase-3: Cleaved Caspase-3

knockdown PLCL1 simultaneously in podocyte of *db/db* mice. In DOT1L overexpression *db/db* mice, fewer lipid droplets were observed in glomeruli as assessed by Oil Red O staining, and in podocytes as assessed by co-staining of Adipophilin, a specific lipid droplet marker, with Synaptopodin, while PLCL1 silencing diminished this protective role of DOT1L (Fig. 8A). Further, DOT1L overexpression decreased the expression levels of lipogenic enzymes such as fatty acid synthetase (FASN), acetyl-CoA carboxylase 1 (ACC1), and stearoyl-CoA desaturase 1 (SCD1) in renal cortex of *db/db* mice; moreover, carnitine palmitoyl transferase 1 A (CPT1a) and

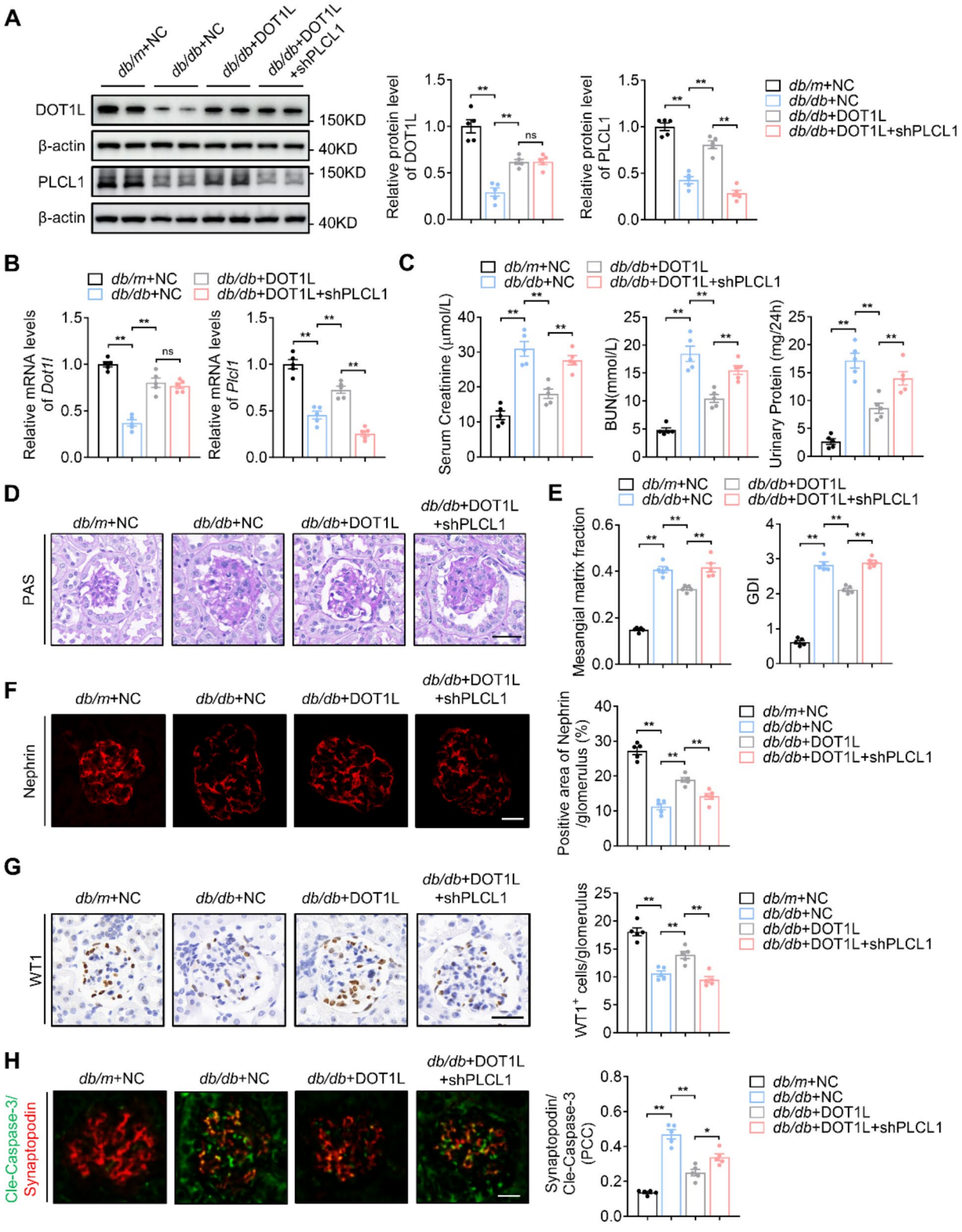

Fig. 6 (See legend on next page.)

(See figure on previous page.)

Fig. 6 DOT1L attenuated podocyte injury under diabetic conditions in PLCL1 dependent way in *db/db* mice. **A** Representative Western blotting and quantification of DOT1L and PLCL1 in renal cortex of mice from different groups at 20 weeks ($n=5$ per groups). **B** The relative mRNA level of *Dot1l* and *Plcl1* in isolated glomeruli ($n=5$ per groups). **C** Serum creatinine, BUN and 24-h urinary protein of mice from different groups ($n=5$ per group). **D** Representative images of morphological changes from periodic acid-Schiff (PAS) staining ($n=5$ per group). Scale bar, 20 μm. **E** Quantification of the percentage of mesangial matrix area and glomerular damage index (GDI) ($n=5$ per group). **F** Representative immunofluorescence staining of Nephrin and the quantitative analysis in mice from different groups ($n=5$ per group). Scale bar, 20 μm. **G** Representative photomicrographs and quantification of WT1 showed the number of podocytes in each glomerular. ($n=5$ per group). Scale bar, 20 μm. **H** Representative immunofluorescence co-staining (yellow) between Synaptopodin (red) and Cle-Caspase-3 (green) and the summarized colocalization coefficient ($n=5$ per group). Scale bar, 20 μm. Data are presented as mean ± SEM. $^{*}P<0.05$, $^{**}P<0.01$. cle-Caspase-3: Cleaved Caspase-3. *db/m* + NC: *db/m* mice + AAV9-Nphs1-NC, *db/db* + NC: *db/db* mice + AAV9-Nphs1-NC, *db/db* + DOT1L: *db/db* mice + AAV9-Nphs1-DOT1L, *db/db* + DOT1L + shPLCL1: *db/db* mice + AAV9-Nphs1-DOT1L + AAV9-Nphs1-shPLCL1

peroxisome proliferator-activated receptor-α (PPARα) expression were restored by DOT1L overexpression. However, by silencing PLCL1, these protective effects were blunted (Fig. 8B and C). Overall, the above results suggest that DOT1L suppresses lipogenesis and stimulates fatty acid oxidation by regulating PLCL1 in diabetes-induced podocytes.

Discussion

In the present study, we demonstrated DOT1L as a novel therapeutic target in diabetes-induced podocyte injury. First, DOT1L expression was significantly reduced in HG-treated podocytes, renal cortex of *db/db* mice, and renal biopsy samples in DKD. Next, in vitro and in vivo studies elucidated that DOT1L overexpression prevented podocyte injury in HG-cultured podocytes and diabetic mice. Mechanistically, RNA-sequencing analysis revealed that PLCL1 was the downstream target of DOT1L. Moreover, DOT1L induced the upregulation of PLCL1 to attenuate the podocyte injury by improving fatty acid metabolism in vitro and in vivo (Fig. 9).

DOT1L has been widely explored and regarded as a new therapeutic target in MLL and other solid tumors by modulating H3K79 methylation [22, 45]. Moreover, previous studies have revealed that DOT1L also acts as a regulator in kidney diseases [30, 32]. We found that DOT1L was down-regulated in HG-treated MPC-5 cells. Meanwhile, DOT1L expression was decreased in podocyte regions of *db/db* mice and renal biopsy samples obtained from diabetic subjects. Since podocyte injury is a critical event during DKD, this study investigates the role of DOT1L in diabetes induced podocyte injury, which remains largely unknown yet.

Zhang *et al*. observed that DOT1L deficiency promotes glomerular sclerosis and interstitial fibrosis in mice with diabetic kidneys [30], suggesting a possible benefit of DOT1L in DKD. To testify whether DOT1L was directly involved in the pathogenesis of podocyte injury under diabetic conditions, we overexpressed DOT1L in MPC-5 cells and in podocytes of *db/db* mice. Here, we demonstrated that DOT1L overexpression attenuated diabetes-induced podocyte injury in vivo and in vitro. Ample evidence has indicated that diabetic deleterious stimuli cause podocyte apoptosis. The anti-apoptotic effect of DOT1L has been reported in some other studies. For instance, DOT1L-KO spermatids exhibited higher apoptosis rates because DOT1L deficiency downregulated anti-apoptotic genes, including *Bcl6*, *Jak3* and *Tsc22d3* [46, 47]. Contrarily, the opposite effect of DOT1L was verified in other studies [48]. This discrepancy may be attributed to the distinct mechanism of DOT1L in diverse disease models. Our study revealed that apoptosis was increased in HG-induced MPC-5 cells and podocytes in *db/db* mice, whereas DOT1L overexpression reversed it. These beneficial effects of DOT1L may be exerted through its modulation of pathways related to apoptosis, which needs further exploration.

To identify the downstream target of DOT1L, RNA sequencing was performed. We employed Western blotting analysis to reveal PLCL1 as DOT1L's lead target candidate protein. Previous studies have reported that DOT1L is enriched in actively transcribing genes and promotes gene expression by catalyzing H3K79 methylation of the promotor [49, 50]. By ChIP analysis, we observed that DOT1L significantly augmented H3K79me2 levels in specific regions of the *Plcl1* promoter, indicating that DOT1L directly induced *Plcl1* expression by epigenetic modification. Moreover, DOT1L overexpression alleviated podocyte injury and apoptosis under diabetic conditions, while PLCL1 depletion abrogated these beneficial effects of DOT1L in vitro and in vivo. Above all, these data suggest that PLCL1 is an unexplored downstream target mediating the protective role of DOT1L in podocytes. However, whether DOT1L would regulate other histone methyltransferases responding to catalyze other residues of histones to promote *Plcl1* transcription in podocytes is warranted to systemically examine in further study.

Increasing data suggests that podocyte lipid metabolism disorder is the main cause of proteinuric kidney disorders, including DKD [39, 40]. DKD patients may benefit from reducing podocyte lipid accumulation, which restores renal function and damage. PLCL1 is a protein homologous to the PLC family and always acts as scaffolding protein involved in numerous pathologic and physiologic processes [51, 52]. Intriguingly, it has been reported that PLCL1 is closely associated with lipid metabolism [42]. Thus, we investigated whether DOT1L

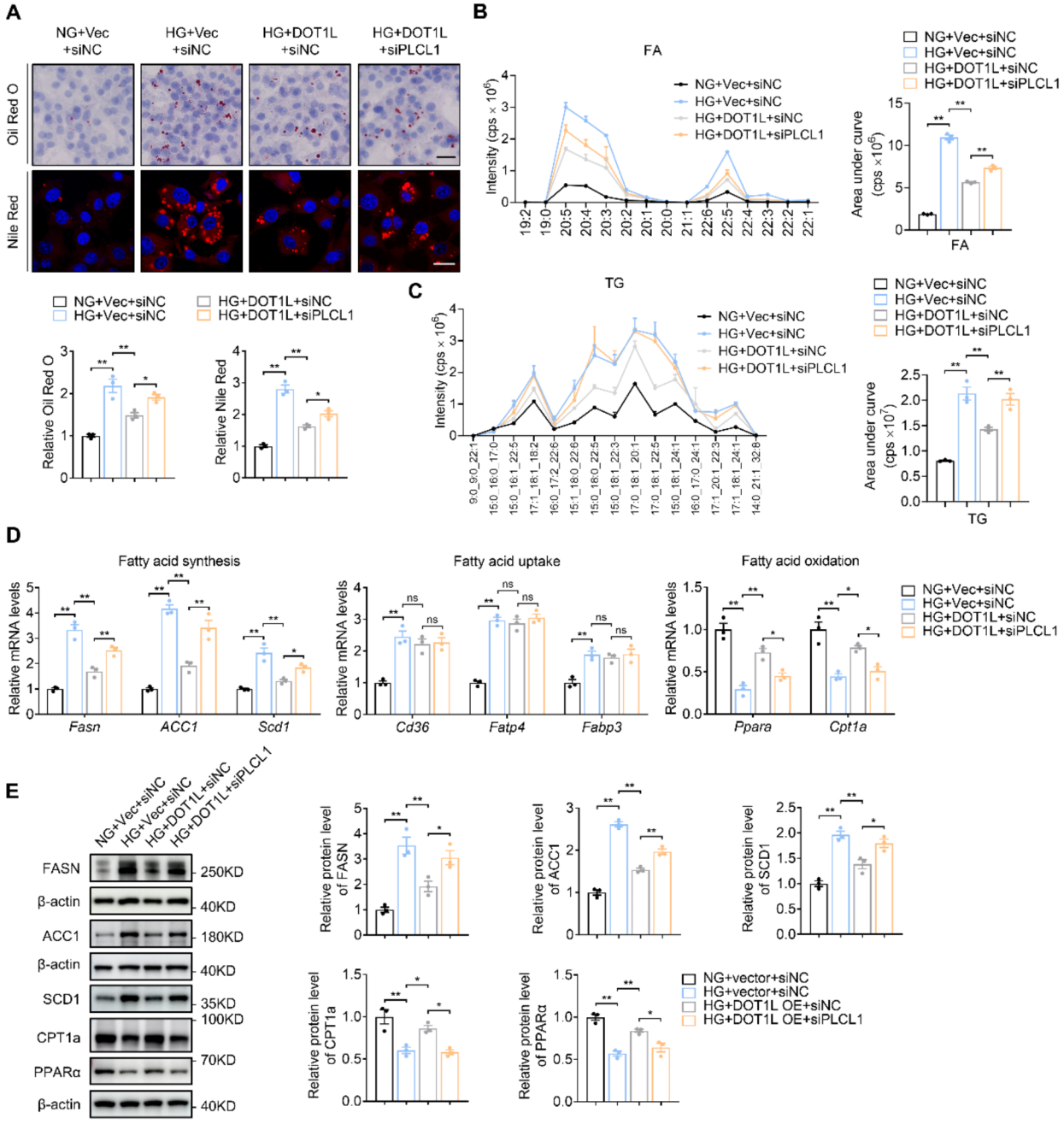

Fig. 7 DOT1L attenuated HG-induced podocytes injury mainly through promoting PLCL1-mediated fatty acid metabolism. **A** Representative images of lipid deposition detected by Oil Red O staining and Nile Red staining and quantification in MPC-5 cells from different groups ($n = 3$ per group). Scale bar, black: 50 μm; white: 20 μm. **B**, **C** UPLC-MS/MS analysis of MPC-5 cells in different groups. Ion chromatograms and quantifications of total lipid content by analysis of AUC of FA (B), and TG (C) in MPC-5 cells ($n = 3$ per group). **D** Relative mRNA levels of key lipogenic genes (*Fasn*, *ACC1*, and *Scd1*), essential fatty acid uptake genes (*Cd36*, *Fatp4* and *Fabp3*), and two crucial oxidation enzymes (*Ppara* and *Cpt1a*) in MPC-5 cells from different groups ($n = 3$ per group). **E** Representative Western blotting and quantification of FASN, ACC1, SCD1, CPT1a, and PPARα in MPC-5 cells from different groups ($n = 3$ per group). Data are presented as mean ± SEM. $^*P < 0.05$, $^{**}P < 0.01$. ns: not significantly different. FA: fatty acid, TG: triglyceride

could regulate podocyte lipid metabolism in PLCL1-dependent way. In our study, DOT1L overexpression inhibited lipid deposition in podocytes under diabetic conditions and PLCL1 silencing blunted this protective effect, showing that PLCL1 was crucial to podocyte lipid metabolism homeostasis mediated by DOT1L. This beneficial effect of DOT1L was further confirmed by lipidomic analysis and we found that the main species of lipid

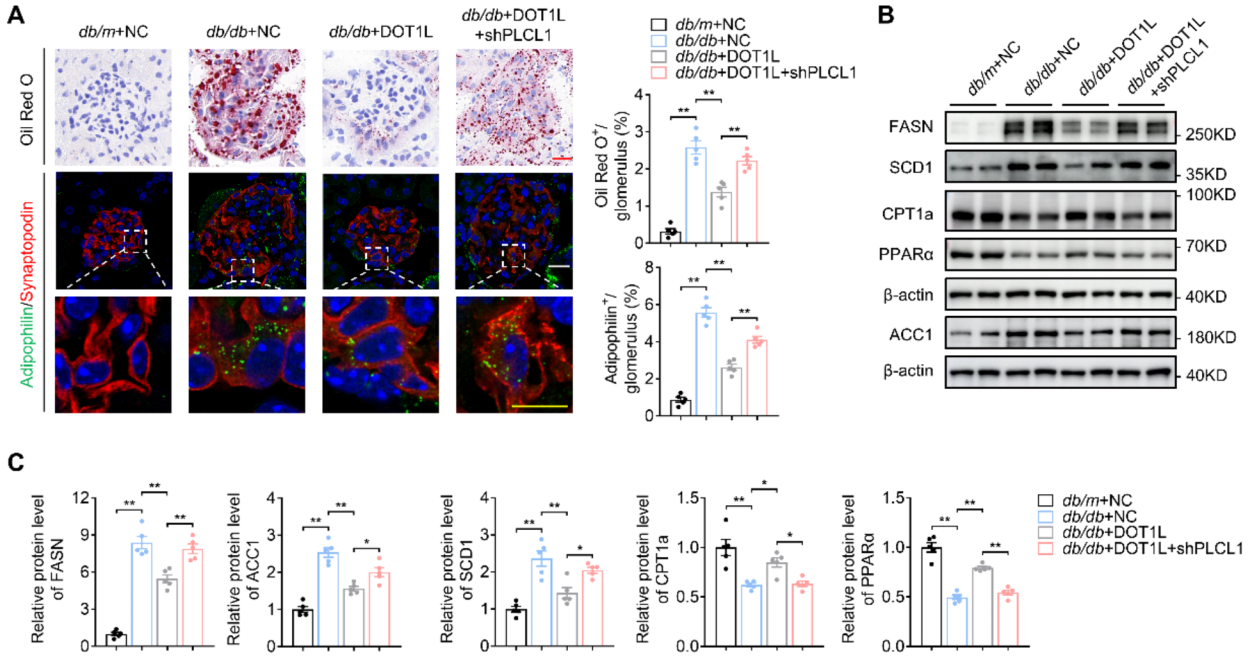

Fig. 8 DOT1L improved podocyte fatty acid metabolism through PLCL1 in *db/db* mice. **A** Representative Oil Red O staining and immunofluorescence images in glomeruli and podocytes (co-staining Adipophilin (green) with Synaptopodin (red)) of mice ($n = 5$ per group). Scale bar, red: 20 μm; white: 20 μm; yellow: 10 μm. **B**, **C** Representative Western blotting and quantification of FASN, ACC1, SCD1, CPT1a, and PPARα in mice from different groups ($n = 5$ per group). Data are presented as mean ± SEM. $^{*}P < 0.05$, $^{**}P < 0.01$. *db/m* + NC: *db/m* mice + AAV9-Nphs1-NC, *db/db* + NC: *db/db* mice + AAV9-Nphs1-NC, *db/db* + DOT1L: *db/db* mice + AAV9-Nphs1-DOT1L, *db/db* + DOT1L + shPLCL1: *db/db* mice + AAV9-Nphs1-DOT1L + AAV9-Nphs1-shPLCL1

regulated by DOT1L/PLCL1 was fatty acid. And we can get some supported information for our results from a recent research. PLCL1 overexpression promotes lipid browning and fatty acid metabolism to repress renal cell carcinoma progression [43]. Disturbance of fatty acid metabolism contributes to podocyte injury caused by diabetes, including apoptosis, fibrosis and so on [53, 54]. Fatty acid metabolism mainly includes the processes of synthesis, uptake and oxidation [44], therefore we assessed the expression of key genes involved in these processes. Our research showed that DOT1L inhibited fatty acid synthesis and promoted oxidation in podocytes. We found that PLCL1 increased the expression of PPARα, a typical regulator for fatty acid uptake genes (such as CD36 and FATP), while CD36 and FATP expression were not affected significantly by PLCL1 silencing, which seemed somewhat contradictory. GW6471 treatment diminished the regulated effecting of PLCL1 on CPT1a, while demonstrating no obvious effect to fatty acid uptake related genes in podocytes with or without PLCL1 knockdown. These data suggest that PLCL1 regulates CPT1a through PPARα, while the process of fatty acid uptake in podocytes may be regulated by alternative pathways besides the PLCL1-PPARα pathway. Though PPARα is a well-known regulator of fatty acid metabolism and regulates the expression of CD36 and FATP, other transcription factors such as PPARγ also participates in maintaining the expression of CD36 and FATP, which may compensate for changes in PPARα levels through alternative pathways [55–58]. Moreover, activation of AMPK promotes the expression of PPARα while decreased the expression of CD36 and FATP in adipose tissues [59]. Taken together, it could be a possibility that PLCL1 regulates the activity of PPARγ or AMPK and offset the effects of PPARα up-regulation on CD36 and FATP after DOT1L overexpression. Further exploration is warranted to elucidate the exact detailed mechanism of how PLCL1 regulates fatty acid metabolism.

Noteworthily, few studies have been conducted on DOT1L involved in lipid metabolism, and the possible role of PLCL1 in diabetes-induced podocyte injury is currently unknown. Taken together, we extended our knowledge of the biological functions of DOT1L in podocyte injury.

Although this study explores the novel biological functions of DOT1L in podocyte injury, as stated above, there are still several limitations worthy of attention. Firstly, further efforts are required to delineate the potential mechanisms by which DOT1L expression is inhibited in podocytes under diabetic conditions. Secondly, while our experiments highlight the activation of PLCL1 in the regulation of podocyte fatty acid metabolism, we cannot

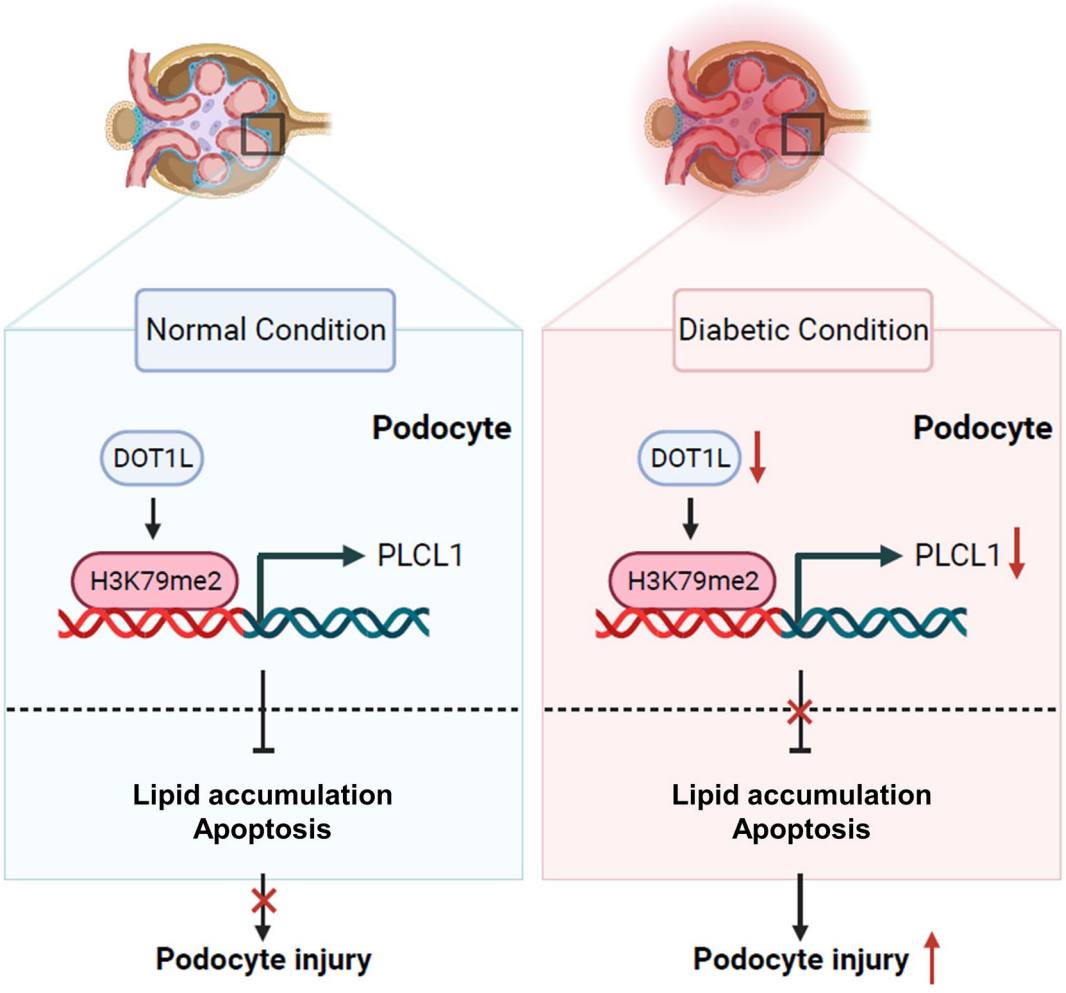

Fig. 9 A model of the molecular mechanism by which DOT1L promotes PLCL1 expression to ameliorate podocyte injury under diabetic conditions. Image created with bioRender.com, with permission

exclude other regulators that may also be involved in this process. Thirdly, in this study we explore the protective role of DOT1L in a PLCL1 dependent way only by the knockdown strategy. Since there are no agonists or inhibitors of PLCL1 in the market at present, we cannot verify our results by pharmacological strategy, which deserves further investigation in the future. Finally, the exact detailed mechanism of how PLCL1 regulates fatty acid metabolism and other potential beneficial effects of PLCL1 in podocytes need further exploration.

Conclusions

Overall, this study shows that DOT1L protects podocytes from diabetic damage through PLCL1 by modulating fatty acid metabolism. Our study opens up potential therapeutic avenues for treating podocyte injury in DKD by targeting DOT1L.

Abbreviations

DKD	Diabetic kidney disease
DOT1L	Disruptor of telomeric silencing 1-like
HG	High glucose
NG	Normal glucose
MA	Mannitol
PLCL1	Phospholipase C-like 1
CKD	Chronic renal disease
ESRD	End-stage renal disease
RAS	Renin-angiotensin system
SGLT2is	Sodium-glucose co-transporter 2 inhibitors
MRA	Mineralocorticoid receptor antagonist
H3K79me	Lysine 79 of histone H3
H3K79me1	Monomethylation of H3K79
H3K79me2	Dimethylation of H3K79
H3K79me3	Trimethylation of H3K79
ChIP	Chromatin immunoprecipitation
BUN	Blood urea nitrogen
BSA	Bovine serum albumin
PFA	Paraformaldehyde
PAS	Periodic-acid-schiff
GDI	Glomerular damage index
FASN	Fatty acid synthetase
ACC1	Acetyl-CoA carboxylase 1
SCD1	Stearoyl-CoA desaturase 1
CPT1a	Carnitine palmitoyl transferase 1 A
PPARα	Peroxisome proliferator-activated receptor-α

Supplementary Information

The online version contains supplementary material available at https://doi.org/10.1186/s12964-024-01895-1.

Supplementary Material 1

Supplementary Material 2

Supplementary Material 3

Acknowledgements
We are grateful for receiving the conditionally immortalized murine podocyte cell line (MPC-5) from Prof. Chun Zhang. We thank Home for Researchers editorial team (http://www.home-for-researchers.com) for language editing service. We appreciate the experimental support from the Medical Research Center, Academy of Chinese Medical Sciences, Zhejiang Chinese Medical University.

Author contributions
CZ and ZDC conceptualized the study. YPH, SY and JK designed the methodology. YPH, SY, JK, QZ, ZW and YQW contributed to the experimental procedures. YPH, SY, JK, TKL, YX, BBC, YMZ and TYZ conducted the analysis. YPH, SY, JK, JJN and BBH generated figures and tables. YPH, SY, JK, XNZ and SYW validated the data. YPH, SY and JK wrote the original draft of the manuscript. CZ, ZDC, YKZ and HY reviewed and edited the manuscript. All authors approved the final version of the manuscript.

Funding
This work was supported by the Natural Science Foundation of Zhejiang Province (LQ23H070003, LQ22H050005, LY22H070001), the National Natural Science Foundation of China (82070833, 82100862, 82370817, 82000767, 82100925, 82100748), Zhejiang Provincial Key Research & Development Program (2021C03070).

Data availability
The datasets used and analyzed during this study are available from the corresponding author on reasonable request.

Declarations

Ethics approval and consent to participate
An informed consent form was signed by all patients in accordance with the Declaration of Helsinki, and the study was approved by the Research Ethics Committee of The Second Affiliated Hospital of Zhejiang University School of Medicine (Approval number: 2023 – 1098). All animal study protocols were approved by the Zhejiang Chinese Medical University's Animal Care Committee (Approval number: 20211206-04).

Consent for publication
Not applicable.

Competing interests
The authors declare no competing interests.

Author details
[1]Department of Endocrinology, The Second Affiliated Hospital of Zhejiang University School of Medicine, 88 Jiefang Road, Hangzhou, Zhejiang, China
[2]Department of Nephrology, The Second Affiliated Hospital, Zhejiang University School of Medicine, 88 Jiefang Road, Hangzhou, Zhejiang, China
[3]Nanjing Kingmed Center for Clinical Laboratory Co., Ltd., 11 Yaogu Avenue, Nanjing, Jiangsu, China
[4]Nursing Department, The Second Affiliated Hospital of Zhejiang University School of Medicine, 88 Jiefang Road, Hangzhou, Zhejiang, China

Received: 10 August 2024 / Accepted: 15 October 2024
Published online: 25 October 2024

References

1. Alicic RZ, Cox EJ, Neumiller JJ, Tuttle KR. Incretin drugs in diabetic kidney disease: biological mechanisms and clinical evidence. Nat Rev Nephrol. 2021;17:227–44.
2. Guedes M, Pecoits-Filho R. Can we cure diabetic kidney disease? Present and future perspectives from a nephrologist's point of view. J Intern Med. 2022;291:165–80.
3. Alicic RZ, Rooney MT, Tuttle KR. Diabetic kidney disease: challenges, Progress, and possibilities. Clin J Am Soc Nephrol. 2017;12:2032–45.
4. Gupta S, Dominguez M, Golestaneh L. Diabetic kidney disease: an update. Med Clin North Am. 2023;107:689–705.
5. Ogurtsova K, da Rocha Fernandes JD, Huang Y, Linnenkamp U, Guariguata L, Cho NH, Cavan D, Shaw JE, Makaroff LE. IDF Diabetes Atlas: global estimates for the prevalence of diabetes for 2015 and 2040. Diabetes Res Clin Pract. 2017;128:40–50.
6. Lytvyn Y, Bjornstad P, van Raalte DH, Heerspink HL, Cherney DZI. The New Biology of Diabetic kidney disease-mechanisms and therapeutic implications. Endocr Rev. 2020;41:202–31.
7. Bakris GL, Agarwal R, Anker SD, Pitt B, Ruilope LM, Rossing P, Kolkhof P, Nowack C, Schloemer P, Joseph A, Filippatos G. FIDELIO-DKD investigators. Effect of Finerenone on chronic kidney Disease outcomes in type 2 diabetes. N Engl J Med. 2020;383:2219–29.
8. Alicic RZ, Johnson EJ, Tuttle KR. SGLT2 inhibition for the Prevention and Treatment of Diabetic kidney disease: a review. Am J Kidney Dis. 2018;72:267–77.
9. Barrera-Chimal J, Lima-Posada I, Bakris GL, Jaisser F. Mineralocorticoid receptor antagonists in diabetic kidney disease - mechanistic and therapeutic effects. Nat Rev Nephrol. 2022;18:56–70.
10. Nagata M. Podocyte injury and its consequences. Kidney Int. 2016;89:1221–30.
11. Lal MA, Patrakka J. Understanding Podocyte Biology to develop novel kidney therapeutics. Front Endocrinol (Lausanne). 2018;9:409.
12. Chen X, Wang J, Lin Y, Liu Y, Zhou T. Signaling pathways of Podocyte Injury in Diabetic kidney Disease and the effect of sodium-glucose cotransporter 2 inhibitors. Cells. 2022;11:3913.
13. Assady S, Wanner N, Skorecki KL, Huber TB. New insights into Podocyte Biology in Glomerular Health and disease. J Am Soc Nephrol. 2017;28:1707–15.
14. Tonneijck L, Muskiet MH, Smits MM, van Bommel EJ, Heerspink HJ, van Raalte DH, Joles JA. Glomerular hyperfiltration in diabetes: mechanisms, clinical significance, and treatment. J Am Soc Nephrol. 2017;28:1023–39.
15. Liu T, Jin Q, Ren F, Yang L, Mao H, Ma F, Wang Y, Li P, Zhan Y. Potential therapeutic effects of natural compounds targeting autophagy to alleviate podocyte injury in glomerular diseases. Biomed Pharmacother. 2022;155:113670.
16. Feng Q, Wang H, Ng HH, Erdjument-Bromage H, Tempst P, Struhl K, Zhang Y. Methylation of H3-lysine 79 is mediated by a new family of HMTases without a SET domain. Curr Biol. 2002;12:1052–8.
17. McGinty RK, Kim J, Chatterjee C, Roeder RG, Muir TW. Chemically ubiquitylated histone H2B stimulates hDot1L-mediated intranucleosomal methylation. Nature. 2008;453:812–6.
18. Steger DJ, Lefterova MI, Ying L, Stonestrom AJ, Schupp M, Zhuo D, Vakoc AL, Kim JE, Chen J, Lazar MA, Blobel GA, Vakoc CR. DOT1L/KMT4 recruitment and H3K79 methylation are ubiquitously coupled with gene transcription in mammalian cells. Mol Cell Biol. 2008;28:2825–39.
19. Takahashi YH, Schulze JM, Jackson J, Hentrich T, Seidel C, Jaspersen SL, Kobor MS, Shilatifard A. Dot1 and histone H3K79 methylation in natural telomeric and HM silencing. Mol Cell. 2011;42:118–26.
20. Kari V, Raul SK, Henck JM, Kitz J, Kramer F, Kosinsky RL, Übelmesser N, Mansour WY, Eggert J, Spitzner M, Najafova Z, Bastians H, Grade M, Gaedcke J, Wegwitz F, Johnsen SA. The histone methyltransferase DOT1L is required for proper DNA damage response, DNA repair, and modulates chemotherapy responsiveness. Clin Epigenetics. 2019;11:4.
21. Daigle SR, Olhava EJ, Therkelsen CA, Majer CR, Sneeringer CJ, Song J, Johnston LD, Scott MP, Smith JJ, Xiao Y, Jin L, Kuntz KW, Chesworth R, Moyer MP, Bernt KM, Tseng JC, Kung AL, Armstrong SA, Copeland RA, Richon VM, Pollock RM. Selective killing of mixed lineage leukemia cells by a potent small-molecule DOT1L inhibitor. Cancer Cell. 2011;20:53–65.
22. Bernt KM, Zhu N, Sinha AU, Vempati S, Faber J, Krivtsov AV, Feng Z, Punt N, Daigle A, Bullinger L, Pollock RM, Richon VM, Kung AL, Armstrong SA. MLL-rearranged leukemia is dependent on aberrant H3K79 methylation by DOT1L. Cancer Cell. 2011;20:66–78.
23. Daigle SR, Olhava EJ, Therkelsen CA, Basavapathruni A, Jin L, Boriack-Sjodin PA, Allain CJ, Klaus CR, Raimondi A, Scott MP, Waters NJ, Chesworth R, Moyer

MP, Copeland RA, Richon VM, Pollock RM. Potent inhibition of DOT1L as treatment of MLL-fusion leukemia. Blood. 2013;122:1017–25.
24. Wong M, Tee AEL, Milazzo G, Bell JL, Poulos RC, Atmadibrata B, Sun Y, Jing D, Ho N, Ling D, Liu PY, Zhang XD, Hüttelmaier S, Wong JWH, Wang J, Polly P, Perini G, Scarlett CJ, Liu T. The histone methyltransferase DOT1L promotes neuroblastoma by regulating gene transcription. Cancer Res. 2017;77:2522–33.
25. Kryczek I, Lin Y, Nagarsheth N, Peng D, Zhao L, Zhao E, Vatan L, Szeliga W, Dou Y, Owens S, Zgodzinski W, Majewski M, Wallner G, Fang J, Huang E, Zou W. IL-22(+)CD4(+) T cells promote colorectal cancer stemness via STAT3 transcription factor activation and induction of the methyltransferase DOT1L. Immunity. 2014;40:772–84.
26. Nassa G, Salvati A, Tarallo R, Gigantino V, Alexandrova E, Memoli D, Sellitto A, Rizzo F, Malanga D, Mirante T, Morelli E, Nees M, Åkerfelt M, Kangaspeska S, Nyman TA, Milanesi L, Giurato G, Weisz A. Inhibition of histone methyltransferase DOT1L silences ERα gene and blocks proliferation of antiestrogen-resistant breast cancer cells. Sci Adv. 2019;5:eaav5590.
27. Zhang X, Liu D, Li M, Cao C, Wan D, Xi B, Li W, Tan J, Wang J, Wu Z, Ma D, Gao Q. Prognostic and therapeutic value of disruptor of telomeric silencing-1-like (DOT1L) expression in patients with ovarian cancer. J Hematol Oncol. 2017;10:29.
28. Vatapalli R, Sagar V, Rodriguez Y, Zhao JC, Unno K, Pamarthy S, Lysy B, Anker J, Han H, Yoo YA, Truica M, Chalmers ZR, Giles F, Yu J, Chakravarti D, Carneiro B, Abdulkadir SA. Histone methyltransferase DOT1L coordinates AR and MYC stability in prostate cancer. Nat Commun. 2020;11:4153.
29. Wang F, Ngo J, Li Y, Liu H, Chen CH, Saifudeen Z, Sequeira-Lopez MLS, El-Dahr SS. Targeted disruption of the histone lysine 79 methyltransferase Dot1L in nephron progenitors causes congenital renal dysplasia. Epigenetics. 2021;16:1235–50.
30. Zhang L, Chen L, Gao C, Chen E, Lightle AR, Foulke L, Zhao B, Higgins PJ, Zhang W. Loss of histone H3 K79 methyltransferase Dot1l facilitates kidney fibrosis by Upregulating Endothelin 1 through histone deacetylase 2. J Am Soc Nephrol. 2020;31:337–49.
31. Yang C, Chen Z, Yu H, Liu X. Inhibition of Disruptor of Telomeric silencing 1-Like alleviated renal ischemia and Reperfusion Injury-Induced fibrosis by blocking PI3K/AKT-Mediated oxidative stress. Drug Des Devel Ther. 2019;13:4375–87.
32. Liu L, Zou J, Guan Y, Zhang Y, Zhang W, Zhou X, Xiong C, Tolbert E, Zhao TC, Bayliss G, Zhuang S. Blocking the histone lysine 79 methyltransferase DOT1L alleviates renal fibrosis through inhibition of renal fibroblast activation and epithelial-mesenchymal transition. FASEB J. 2019;33:11941–58.
33. Ma H, Togawa A, Soda K, Zhang J, Lee S, Ma M, Yu Z, Ardito T, Czyzyk J, Diggs L, Joly D, Hatakeyama S, Kawahara E, Holzman L, Guan JL, Ishibe S. Inhibition of podocyte FAK protects against proteinuria and foot process effacement. J Am Soc Nephrol. 2010;21:1145–56.
34. Chen H, Huang Y, Zhu X, Liu C, Yuan Y, Su H, Zhang C, Liu C, Xiong M, Qu Y, Yun P, Zheng L, Huang K. Histone demethylase UTX is a therapeutic target for diabetic kidney disease. J Physiol. 2019;597:1643–60.
35. Lei C, Li M, Qiu Y, Xie Y, Hao Z, Yin X, Zhang Z, Su H, Yang L, Lin J, Hammes HP, Zhang C. Asparaginyl endopeptidase protects against podocyte injury in diabetic nephropathy through cleaving cofilin-1. Cell Death Dis. 2022;13:184.
36. Wang Z, Chen Z, Wang X, Hu Y, Kong J, Lai J, Li T, Hu B, Zhang Y, Zheng X, Liu X, Wang S, Ye S, Zhou Q, Zheng C. Sappanone a prevents diabetic kidney disease by inhibiting kidney inflammation and fibrosis via the NF-κB signaling pathway. Front Pharmacol. 2022;13:953004.
37. Chen Z, Wang Z, Hu Y, Lin H, Yin L, Kong J, Zhang Y, Hu B, Li T, Zheng X, Yang Q, Ye S, Wang S, Zhou Q, Zheng C. ELABELA/APJ Axis prevents Diabetic glomerular endothelial Injury by regulating AMPK/NLRP3 pathway. Inflammation. 2023;46:2343–58.
38. Fan Y, Yang Q, Yang Y, Gao Z, Ma Y, Zhang L, Liang W, Ding G. Sirt6 suppresses high glucose-Induced mitochondrial dysfunction and apoptosis in Podocytes through AMPK activation. Int J Biol Sci. 2019;15:701–13.
39. Fu Y, Sun Y, Wang M, Hou Y, Huang W, Zhou D, Wang Z, Yang S, Tang W, Zhen J, Li Y, Wang X, Liu M, Zhang Y, Wang B, Liu G, Yu X, Sun J, Zhang C, Yi F. Elevation of JAML promotes Diabetic kidney disease by modulating podocyte lipid metabolism. Cell Metab. 2020;32:1052–e10628.
40. Mitrofanova A, Merscher S, Fornoni A. Kidney lipid dysmetabolism and lipid droplet accumulation in chronic kidney disease. Nat Rev Nephrol. 2023;19:629–45.
41. Wu M, Yang Z, Zhang C, Shi Y, Han W, Song S, Mu L, Du C, Shi Y. Inhibition of NLRP3 inflammasome ameliorates podocyte damage by suppressing lipid accumulation in diabetic nephropathy. Metabolism. 2021;118:154748.
42. Okumura T, Harada K, Oue K, Zhang J, Asano S, Hayashiuchi M, Mizokami A, Tanaka H, Irifune M, Kamata N, Hirata M, Kanematsu T. Phospholipase C-related catalytically inactive protein (PRIP) regulates lipolysis in adipose tissue by modulating the phosphorylation of hormone-sensitive lipase. PLoS ONE. 2014;9:e100559.
43. Xiong Z, Xiao W, Bao L, Xiong W, Xiao H, Qu Y, Yuan C, Ruan H, Cao Q, Wang K, Song Z, Wang C, Hu W, Ru Z, Tong J, Cheng G, Xu T, Meng X, Shi J, Chen Z, Yang H, Chen K, Zhang X. Tumor Cell Slimming regulates Tumor Progression through PLCL1/UCP1-Mediated lipid Browning. Adv Sci (Weinh). 2019;6:1801862.
44. Opazo-Ríos L, Mas S, Marín-Royo G, Mezzano S, Gómez-Guerrero C, Moreno JA, Egido J. Lipotoxicity and Diabetic Nephropathy: Novel mechanistic insights and Therapeutic opportunities. Int J Mol Sci. 2020;21:2632.
45. Anglin JL, Song Y. A medicinal chemistry perspective for targeting histone H3 lysine-79 methyltransferase DOT1L. J Med Chem. 2013;56:8972–83.
46. Ishiguro K, Kitajima H, Niinuma T, Ishida T, Maruyama R, Ikeda H, Hayashi T, Sasaki H, Wakasugi H, Nishiyama K, Shindo T, Yamamoto E, Kai M, Sasaki Y, Tokino T, Nakase H, Suzuki H. DOT1L inhibition blocks multiple myeloma cell proliferation by suppressing IRF4-MYC signaling. Haematologica. 2019;104:155–65.
47. Shan L, Hao C, Jun Z, Qinghe C. Histone methyltransferase Dot1L inhibits pancreatic cancer cell apoptosis by promoting NUPR1 expression. J Int Med Res. 2022;50:3000605221088431.
48. Wang J, Zhong W, Su H, Xu J, Yang D, Liu X, Zhu YZ. Histone methyltransferase Dot1L contributes to RIPK1 kinase-dependent apoptosis in cerebral Ischemia/Reperfusion. J Am Heart Assoc. 2021;10:e022791.
49. Nguyen AT, Zhang Y. The diverse functions of Dot1 and H3K79 methylation. Genes Dev. 2011;25:1345–58.
50. Wood K, Tellier M, Murphy S. DOT1L and H3K79 methylation in transcription and genomic Stability. Biomolecules. 2018;8:11.
51. Uji A, Matsuda M, Kukita T, Maeda K, Kanematsu T, Hirata M. Molecules interacting with PRIP-2, a novel ins(1,4,5)P3 binding protein type 2: comparison with PRIP-1. Life Sci. 2002;72:443–53.
52. Fujii M, Kanematsu T, Ishibashi H, Fukami K, Takenawa T, Nakayama KI, Moss SJ, Nabekura J, Hirata M. Phospholipase C-related but catalytically inactive protein is required for insulin-induced cell surface expression of gamma-aminobutyric acid type A receptors. J Biol Chem. 2010;285:4837–46.
53. Chen Q, Xie C, Tang K, Luo M, Zhang Z, Jin Y, Liu Y, Zhou L, Kong Y. The E3 ligase Trim63 promotes podocyte injury and proteinuria by targeting PPARα to inhibit fatty acid oxidation. Free Radic Biol Med. 2023;209:40–54.
54. Li YJ, Chen X, Kwan TK, Loh YW, Singer J, Liu Y, Ma J, Tan J, Macia L, Mackay CR, Chadban SJ, Wu H. Dietary Fiber protects against Diabetic Nephropathy through short-chain fatty acid-mediated activation of G protein-coupled receptors GPR43 and GPR109A. J Am Soc Nephrol. 2020;31:1267–81.
55. Nakamura MT, Yudell BE, Loor JJ. Regulation of energy metabolism by long-chain fatty acids. Prog Lipid Res. 2014;53:124–44.
56. Miao Y, Zhang C, Yang L, Zeng X, Hu Y, Xue X, Dai Y, Wei Z. The activation of PPARγ enhances Treg responses through up-regulating CD36/CPT1-mediated fatty acid oxidation and subsequent N-glycan branching of TβRII/IL-2Rα. Cell Commun Signal. 2022;20:48.
57. Frohnert BI, Hui TY, Bernlohr DA. Identification of a functional peroxisome proliferator-responsive element in the murine fatty acid transport protein gene. J Biol Chem. 1999;274:3970–7.
58. Liu S, Zhang H, Li Y, Zhang Y, Bian Y, Zeng Y, Yao X, Wan J, Chen X, Li J, Wang Z, Qin Z. S100A4 enhances protumor macrophage polarization by control of PPAR-γ-dependent induction of fatty acid oxidation. J Immunother Cancer. 2021;9:e002548.
59. Cao Q, Zhang J, Yu Q, Wang J, Dai M, Zhang Y, Luo Q, Bao M. Carotid baroreceptor stimulation in obese rats affects white and brown adipose tissues differently in metabolic protection. J Lipid Res. 2019;60:1212–24.

Publisher's note